Master's thesis

NTNU
Norwegian University of Science and Technology
Faculty of Natural Sciences
Department of Biotechnology and Food Science

Ingrid Weløy Aarseth

Bioprinting of functionalized alginate-nanocellulose scaffolds for 3D cultivation of human dermal fibroblasts

Master's thesis in Biotechnology
Supervisor: Øystein Arlov and Berit Løkensgard Strand
Co-supervisor: Aman S. Chahal
May 2022

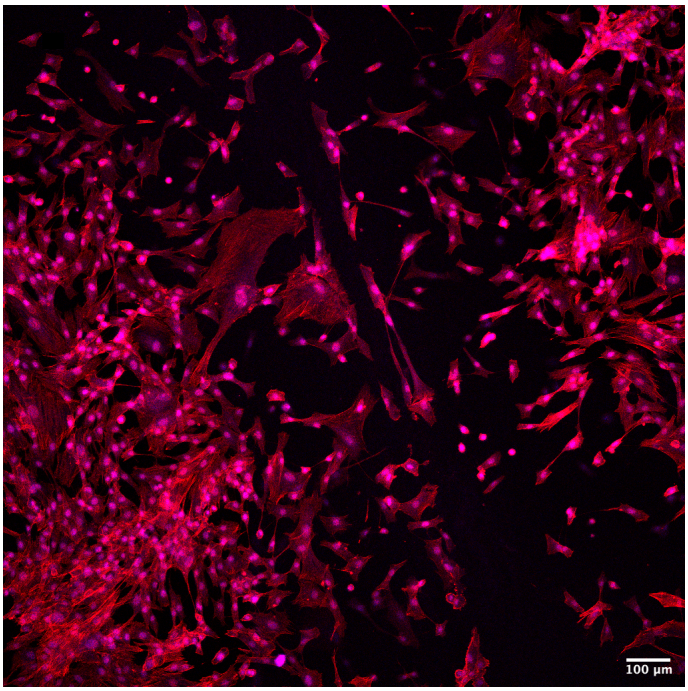

NTNU
Kunnskap for en bedre verden

Ingrid Weløy Aarseth

Bioprinting of functionalized alginate-nanocellulose scaffolds for 3D cultivation of human dermal fibroblasts

Master's thesis in Biotechnology
Supervisor: Øystein Arlov and Berit Løkensgard Strand
Co-supervisor: Aman S. Chahal
May 2022

Norwegian University of Science and Technology
Faculty of Natural Sciences
Department of Biotechnology and Food Science

NTNU
Kunnskap for ei betre verd

Acknowledgements

This master's thesis was completed at the Department of Biotechnology and Food Science at the Norwegian University of Science and Technology (NTNU) from August 2021 to May 2022, in collaboration with SINTEF Industry as part of the NTNU and SINTEF project 3DLife. Prior to starting the master's thesis, I was awarded the SINTEF scholarship to attend the RegenHU Bioprinting Academy. This provided me with a solid understanding of the 3D-bioprinter and which parameters to use for my materials.

I would like to express gratitude to my supervisor, Øystein Arlov, for giving me the opportunity to work on this thesis and for the invaluable guidance throughout this year. Many thanks to my co-supervisor Aman S. Chahal for your engagement, as well as your insights and guidance in the cell work that was completed. Thank you to Berit Løkensgard Strand for the coordination of this project. I would also like to express my appreciation to everyone at the SINTEF Industry laboratory. I was made to feel welcome and included in the work environment. An extra thank you to Andrea Draget Hoel, Trine Muren, Anita Akbarzadeh and Susan Maleki for helping me with laboratory methods within cell work, rheology, and carbon filtration. Thank you to my fellow master's office students for being engaged in each other's work, especially Nikki, who helped me with English grammar and taught me how to do a cartwheel.

Finally, I want to thank my family, friends, and Øyvind for always encouraging me and being just a phone call away.

Trondheim, May 16th, 2022

Ingrid Weløy Aarseth

Abstract

Novel systems for 3D-cell cultivation have been extensively researched to provide better *in vitro* microenvironments for cells. The goal of such systems is to create physiologically representative cell cultures to investigate microenvironments for cells, and to establish tissues that can be used in cancer and drug research. 3D-bioprinting has been used to create custom-made scaffolds with encapsulated or seeded cells, but the formulation of a bioink that is biocompatible and has suitable structuring properties is one of the critical challenges for the clinical application of 3D-bioprinting. The main objective of this study was to develop and characterize novel bioinks composed of functionalized alginates and nano fibrillated cellulose that had mechanical properties suitable for 3D-bioprinting and were biocompatible with human dermal fibroblasts.

Rheological measurements were conducted to characterize the biomaterials. Measured flow curves demonstrated that the alginates with the highest viscosities also were quantitatively observed as favourable for subsequent bioink formulation. Bioinks composed of TTC/alginate ratios at 70/30 and 80/20 demonstrated great printability and produced homogeneous filaments with high stability before and after crosslinking. The bioinks were further investigated in cell-biomaterial interaction studies where viability, morphology, and adhesion of dermal fibroblasts were analysed by CLSM. Regardless of present RGD, all formulated bioinks were biocompatible for encapsulated cells, demonstrating cell viability above 70%. Significantly higher numbers of seeded cells adhered to RGD-coupled bioinks compared to negative controls. When RGD was present, no clear differences in cell adhesion were seen on either alginate or ratio used. Therefore, alginates with high molecular weight and high G-content allowed flexibility in bioink formulations and should be further investigated for use in tissue engineering and 3D-bioprinting.

Sammendrag

Nye systemer for 3D-cellekultivering har blitt forsket på for å forbedre *in vitro* mikromiljø for celler. Målet til disse systemene er å danne et fysiologisk representativt miljø for cellekulturer slik at man kan undersøke mikromiljø og etablere vev som kan bli brukt i forskning på kreft og utvikling av medisiner. 3D-bioprinting har blitt brukt til å lage spesialtilpassede vekststillas som enten har innkapslede celler i seg eller har blitt sådd med celler på utsiden. En stor utfordring for klinisk bruk av 3D-bioprinting er formuleringen av et bioblekk som både er biokompatibelt og har ønskede strukturelle egenskaper. Hovedmålet med denne oppgaven var derfor å utvikle og karakterisere nye bioblekk av funksjonalisert alginat og nanofibrillert cellulose med mekaniske egenskaper tilpasset 3D-bioprinting og som i tillegg er biokompatibel med menneskelige dermale fibroblaster.

Biomaterialene ble karakterisert med reologiske målinger. Målte flytkurver viste at alginater med høy viskositet også var kvantitativt ansett som gunstige for videre bruk i bioblekk formulering. Bioblekk dannet av TTC/alginat mengdeforhold på 70/30 og 80/20 demonstrerte god printbarhet og produserte homogene filamenter med høy stabilitet både før og etter de var kryssbundet. Bioblekkene ble videre undersøkt i celle-biomaterial interaksjonsstudier hvor celleoverlevelse, morfologi og adhesjon av dermale fibroblaster ble analysert med CLSM. Alle bioblekkene var biokompatible for innkapslede celler ettersom en celleoverlevelse på over 70% var registrert uavhengig om RGD var til stede. Et signifikant høyere antall celler hadde festet seg til bioblekk med RGD-koblet alginat sammenlignet med negative kontroller. Når RGD var til stede ble ingen store forskjeller mellom de ulike alginatene eller mengdeforholdene observert. Alginater med høy molekylvekt og høyt G-innhold ga derfor en fleksibilitet under bioblekk formuleringen og bør bli videre studert for bruk i *in vitro* vevsdannelse og 3D-bioprinting.

Abbreviations

CLSM	Confocal laser scanning microscopy
DAPI	4’,6-diamidino-2-phenylindole
DMEM	Dulbecco´s Modified Eagle Medium
ECM	Extracellular matrix
FBS	Fetal bovine serum
FGF	Fibroblast growth factor
G	α-L-guluronic acid
G’	Elastic shear modulus
G’’	Viscous shear modulus
GRGDSP	Glycine-Arginyl-Glycine-Aspartic-Serine-Proline
HG LM_w	High-G, low-molecular-weight bacterial alginate
HG HM_w	High-G, high-molecular-weight bacterial alginate
LHS LM_w	Laminaria hyperborea stipe low molecular weight alginate
LHS HM_w	Laminaria hyperborea stipe high molecular weight alginate
LVR	Linear viscoelastic region
M	β-D-mannuronic acid
NFC	Nano Fibrillated Cellulose
NHDF	Normal Human Dermal Fibroblasts
PH1	Inkjet printhead CF300H
PH3	Extrusion based printhead by velocity control HPD-100
PH4	Extrusion based printhead with air pressure DD-135H
PSS	Physiological saline solution
RGD	Arginyl-glycyl-aspartic acid
TTC	TEMPO-mediated oxidized tunicate nanocellulose
TTC+M	Medical grade TEMPO-mediated oxidized tunicate nanocellulose
UPLVG	Ultra-pure low viscosity sodium alginate with high guluronic acid
w/v	Weight/volume
δ	Phase angle

Table of contents

1. Introduction

1.1 *In vitro* cell and tissue models

In vitro cell models are extensively used in medicine and biology to get an insight into cell behaviour and cell properties (1). The well-established and thoroughly investigated 2D cultivation of cells on glass or polystyrene have provided invaluable insights into cellular functions and drug research. However, the 2D cultivation method has been criticized because cell monolayers do not provide a correct representation of the cells found in the extracellular matrix (ECM) (2). As a result, drugs tested on 2D cultivated cells have low clinical trial success rates, with more than half of the tested drugs failing in Phase II and Phase III (3). Animal models, on the other hand, are used to test drugs *in vivo* and are still considered an essential disease model (4) but have been criticized for producing inaccurate results for drugs developed for humans. Furthermore, ethical concerns have been raised about the discomfort and pain caused to living subjects (5). Several different 3D cell cultivation methods have been investigated to bridge the gap between cellular monolayers and the use of animal models (2). These can be divided into three main systems; scaffold-free, scaffold-based and hybrid systems which are being developed for different applications (4). Figure 1 shows an overview of some of these systems.

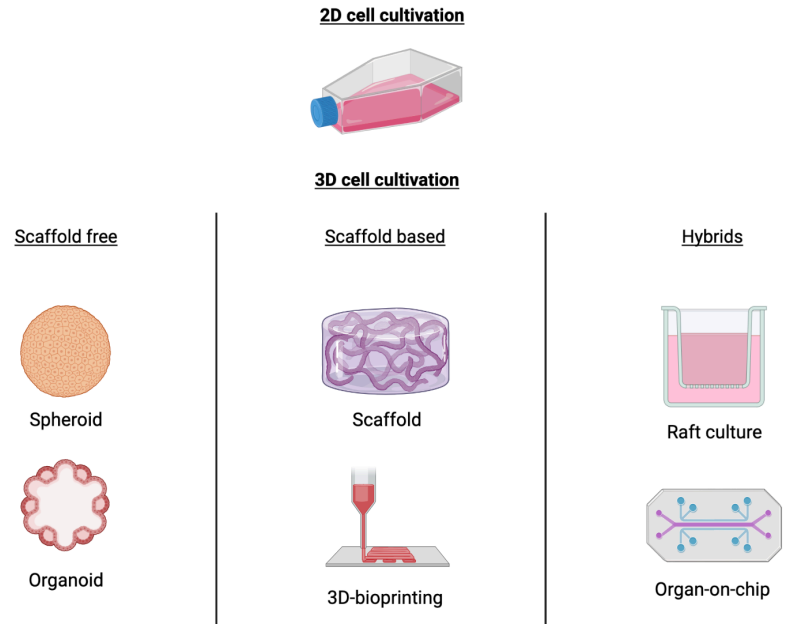

Figure 1 Overview of different 3D-cell cultivation strategies. Created in Biorender.com, adapted from (4).

All systems aim to provide the cells with a more realistic environment, causing them to behave more like they would *in vivo* (4). An accurate reproduction of the tissues in question is critical for drug screenings and tissue biology studies (6). Scaffold free systems and hybrid systems are often employed and investigated in cancer research and drug testing (4). In tissue engineering, where the goal is to restore or build tissues (6), the implantation of functional tissues for regeneration may only necessitate the use of temporary biodegradable scaffolds. This allows the body to reorganize and replace the implanted tissue with native tissue over time (2).

1.1.1 Chemical functionalization of hydrogels and the extracellular matrix

Natural and synthetic hydrogels are extensively used as scaffolds in tissue engineering. Their polymer networks can hold large amounts of water and allow soluble growth-enhancing factors to diffuse through the tissue-like gels (7). Differentiation, gene expression and cell fate are influenced by the surface topography of the hydrogel (8) and the adhesion to a substrate is crucial for cell types like epithelial, endothelial, and muscle cells which without attachment will undergo apoptosis (9). Hydrogels derived from animal sources such as Matrigel, collagen and fibrin contain natural adhesion proteins and growth factors which give a great base for cell proliferation and tissue formation (10). However, these hydrogels have their limitations such as high batch-to-batch variation, high immunogenicity and potential risks for pathogen-transmission (11). When purified, hydrogels like alginate, chitosan, and agarose do not elicit these immunological responses (12). However, they lack natural surface proteins that interact with living cells. This can be remedied by modifying or functionalizing them to mimic the properties of the native extracellular matrix (8).

The extracellular matrix (ECM) is a complex dynamic network formed when eukaryotic cells interact with each other and extracellular macromolecules to establish tissue. There is a bi-directional physical and chemical relationship (13) where the cells make, organize and degrade the ECM while the ECM influences their architectural structure, mechanical properties and chemical composition (8). The ECM is built up of glycosaminoglycans (GAGs), fibrous proteins and glycoproteins which allow communication between cells and the ECM. Matrix receptors bind to the cell's cytoskeleton and this mechanical attachment enables components of the matrix to influence cell behaviour (9). This is a highly complex and well-developed chemical and physical network that is difficult to replicate *in vitro*. Rather than striving to create an ECM that is identical to native tissues, tissue engineering scientists have created suitable conditions for cells to encourage the formation of new tissues based on key components from

the ECM (2). One of these key components is the integrins. Integrins are transmembrane proteins under the glycoprotein family and the primary receptors on animal cells for binding most extracellular matrix proteins. They are composed of two subunits called α and β which bind to the specific amino acid sequence RGD (Arginine-Glycine-Aspartate) found on other cells or proteins in the ECM. Integrins transmit or convert molecular and mechanical signals both in and out of the plasma membrane and are crucial for the adhesion to a substrate (9). To make hydrogels more compatible with living cells can therefore synthetically produced RGD be used to functionalize them (8).

1.1.2 Normal Human Dermal Fibroblasts

Fibroblasts are an important member of the connective-tissue cell family. They are distinguished by their flat, spindle-shaped morphology and specialize in the secretion of collagenous ECM. They have a high rate of proliferation in wound healing where they migrate to the injured tissue and produce a collagenous matrix. Since they are easy to grow in cultures and have high activity in wound healing are they frequently used in tissue engineering (9).

Normal human dermal fibroblasts (NHDF) are unmodified cells isolated from the second skin layer of adult skin or neonatal foreskin (14). Because they are isolated directly from the tissue are they classified as primary cells which have low mutation rates but a short life span (15). They rely on adhesion for survival and typically divide only 35-40 times in culture before dying (9). Cell-derived ECM has been used to investigate NHDF properties when cultivated in 3D which revealed a great difference in cell behaviour compared to 2D cultivated cells. When cultivated in 3D, the cells proliferated twice as fast and had improved cell adhesion. The morphology was also altered, as they resembled *in vivo* cells with elongated and spindle-shaped morphology, whereas the 2D cultivated cells had fan-shaped lamellae (16).

1.1.3 Cell characterization

Cytotoxicity and cell viability assays are frequently used to assess how the microenvironment affects cells. These assays can be based on a variety of cellular functions wherein particular proteins are labelled with dye or fluorescence. Cell number, viability, and metabolic activity can then be assessed depending on the presence of the labels (17). Confocal laser scanning microscopy (CLSM) is ideal for quantitative measurements of cell distribution, morphology, and viability in 3D cell cultures. By using laser beams fluorescence labelled proteins are excited

and the CLSM gives the ability to evaluate samples in X, Y, and Z directions. To capture the structure of interest are several confocal images captured to produce z-stacks (a 3D dataset) which can be merged into one image, or rendered as a 3D-image (18).

1.2 3D-bioprinting

Three dimensional (3D) bioprinting is an emerging technology used to dispense biocompatible materials and cells layer-by-layer at a micrometre precision. The 3D-bioprinting fabrication technology is highly advanced and enables the creation of complex and detailed structures by dispensing biomaterials in X, Y and Z directions (19). This is directed by software where a 3D-model of the wanted structure is designed and translated to commands related to movement, extrusion, and other functionalities. A printhead loaded with bioink will then be directed to print the envisaged model. Extrusion, inkjet, and laser-aided printing are the three primary 3D-bioprinting methods, these are based on different principles and are illustrated in Figure 2. Extrusion printing dispenses bioink loaded in a syringe as a filamentous strand and is dependent on nozzle size and shape, and the force applied. The dispersion is accomplished using either air pressure or mechanical force where the bioink is guided by a screw or piston. In inkjet bioprinting, cell loaded bioinks are dispersed drop by drop by either electric signals, microvalve or thermal action. Inkjet bioprinting can be alleviated by LASER-aided bioprinting. When the LASER is activated, it will indirectly interact with the cell loaded bioink by heat and pulsation and guide the droplets at a high velocity (20-100 m/s) in a predefined track (20). The extrusion-based bioprinting is the widespread method used in the medical field due to its rapid and convenient fabrication of porous 3D cellular structures (10).

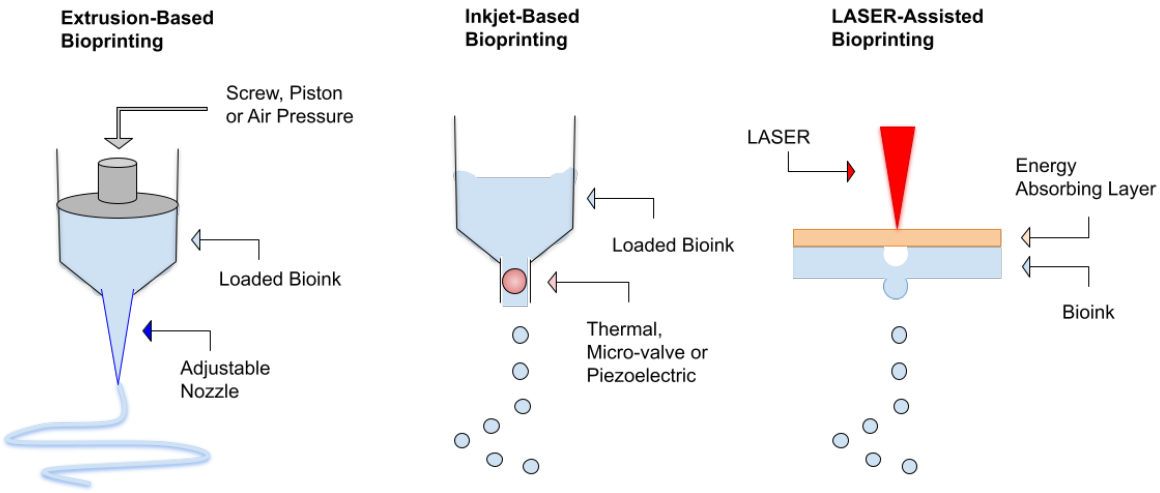

Figure 2 Illustration of the three main bioprinting principles. Adapted from (21).

Spatial bioink deposition enables 3D-bioprinting to create scaffolds with external geometry that mimics the tissue or organ to be repaired. Thereby, 3D-bioprinting can be used in tissue engineering to create custom structures to fill defects and replicate native tissues. Cells can either be incorporated into the scaffold before printing or seeded onto the scaffold after printing. Access of the encapsulated cells to the surrounding medium is improved by printing scaffolds with porous internal structures and increasing the surface area of the hydrogels (22). 3D-bioprinting also allows for controlled deposition of multiple cell types and biomaterials in advanced co-cultures (23). As a result, 3D-bioprinting is applied to fabricate tissues for research in a variety of applications. It can be used to increase the understanding of cell-biomaterial interactions, produce cell-biomaterial grafts for tissue replacement, and create artificial tissues for cell-based sensors and drug screening (19, 24).

The bioinks must be suitable for living cells while also being viscous enough to be printed and retain their intended structure until they are crosslinked in a non-toxic manner (19, 24). Their mechanical strength following crosslinking is also important because it must be strong enough to maintain its structure until the cells have established themselves sufficiently to produce ECM while also being degradable and allowing native tissue to eventually replace it (22). The development of bioinks with good structuring properties while ensuring a cell-compatible and stimulating environment is a critical challenge in the realization of 3D-bioprinting in clinical applications (19, 24).

1.3 Alginate

Alginate is a family of natural polysaccharides that can be chemically extracted from the cell walls and intracellular spaces of brown algae or be produced by specific bacteria strains via fermentation (25). It makes up around 30-40% of the dry weight in brown algae and is an important structural component that provides both flexibility and mechanical strength which protect it from its natural surroundings. The soil bacteria strain *Pseudomonas* and *Azotobacter* have several species that produce capsular polysaccharides similar to the alginate from brown algae (26). Commercial alginates are derived from brown seaweeds because they are easily harvested in large quantities from nature. *Laminaria hyperborea* and *Laminaria digitata* are sources of most commercially produced alginates. Microbially produced alginates, on the other hand, are currently not economically feasible to produce for commercial use (25) but have promising potential as industrial polymers (27).

1.3.1 Chemical structure

Alginate is a linear polysaccharide built up of the two monomers α-L-guluronic acid (G) and β-D-mannuronic acid (M). The biosynthesis begins with the polymerization of the precursor molecule GDP-D-mannuronic acid, where enzymes such as transferase form linkages between carbon 1 and 4 resulting in the formation of long chains of M. The extracellular enzyme epimerase will attack carbon 5 and reverse the carboxyl group (-COOH). This reaction alters the molecule´s configuration and produces a new sugar, the epimer of carbon 5. This is known as an L-sugar or the α-L-guluronic acid (G). The various structures of alginates are due to different epimerases introducing different patterns of G, alginates are therefore composed of M-, G- and MG-blocks of varying lengths (25). Figure 3 shows the different chemical structures of the block compositions. Because of their different alginate compositions, the stem and stipe of seaweeds are commonly separated. *L. hyperborea* stipe demonstrates one of the best gelling alginates as it contains high G/M ratios and long G blocks (25).

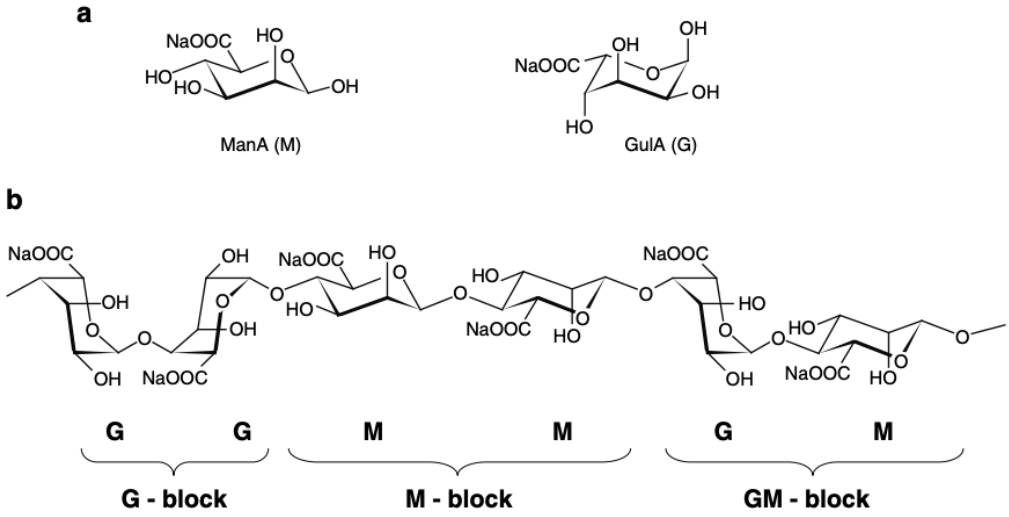

Figure 3 Chemical structure of alginate monomers. **a:** shows the conformation of β-D-mannuronic acid (M) and α-L-guluronic acid (G) **b:** shows the different block compositions of alginate with G-, M- and GM- blocks. Retrieved from (28).

Bacterial alginates have a different chemical structure with some M residues being O-acetylated. These hinder epimerases from reversing the carboxyl group but can be removed by deacetylation in alkaline conditions (29). AlgE is a gene cluster that encodes all the enzymes involved in the biosynthesis of alginate. It is identified and sequenced from both *Pseudomonas* and *Azotobacter* species which enables the possibilities of polysaccharide engineering (26). For example, modifications of *Pseudomonas* have been done to create epimerase-negative mutants which only produce mannuronan chains. Epimerization can then be carried out *in vitro*,

allowing for the creation of sequences that do not exist in nature (27). Epimerization of high-G alginates can be accomplished by using the C5 epimerase enzyme AlgE4 to convert homopolymeric M blocks into copolymeric MG blocks, followed by AlgE6 to produce G blocks, or AlgE1 to introduce both MG and G blocks to the alginate chains (28). The chemical modifications made by the three enzymes are illustrated in Figure 4.

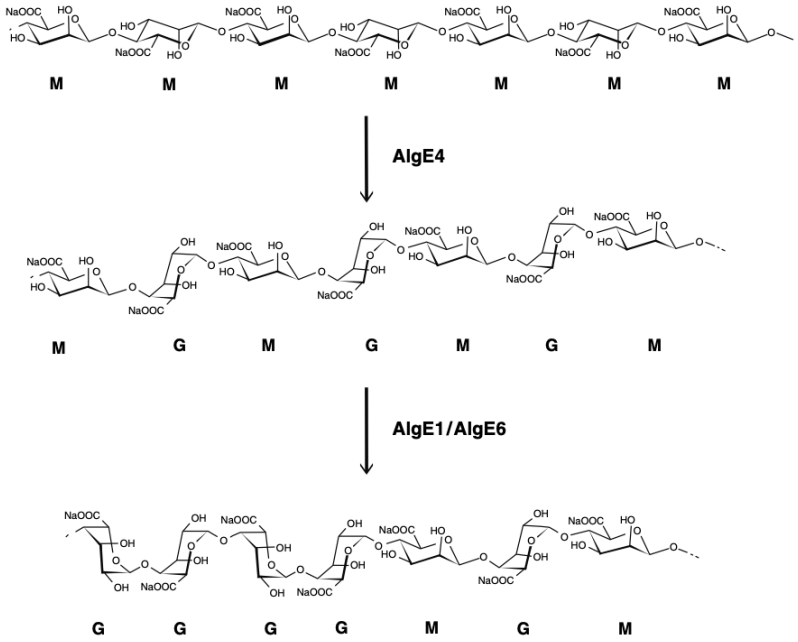

Figure 4 Epimerization of alginate. The epimerase AlgE4 converts mannuronan into poly alternating alginate. In a second reaction step, AlgE1 or AlgE6 are used to introduce G-blocks along the polysaccharide chain. Retrieved from (28).

1.3.2 Alginate hydrogels

Gelation of alginate is based on the selective binding of specific ions. When longer G-blocks on alginate chains are exposed to divalent cations such as calcium (Ca^{2+}), barium (Ba^{2+}), magnesium (Mg^{2+}) or strontium (Sr^{2+}), they crosslink with G-blocks in other alginate chains and form a three-dimensional polymer network (25). This hydrophilic crosslinked network of alginate gives it comparable properties to the extracellular matrix found in human tissues (19). The mechanical properties of the crosslinked gel are therefore strictly linked to the length and number of G-blocks in the polysaccharide, as well as the alginate chain length (27). Crosslinking alginates with Ca^{2+} is widely used in biofabrication because it is a milder crosslinking agent for cells than crosslinking with changes in temperature, pH, or UV (20). Crosslinking can be performed using a diffusional setting which involves the addition of Ca^{2+} around the hydrogel where the ions diffuse into the alginate solution (27), or by internal gelation

where $CaCO_3$ is mixed in the alginate solution and Ca^{2+} ions are released in the interior when pH is lowered (30).

Endotoxins, heavy metals, and polyphenols are removed when alginates are purified. These impurities are immunogenic, and purification lowers the risk of immunologic reactions when alginate is transplanted into a host. Because humans lack the alginate lyase enzyme, which cleaves polymer chains, crosslinked alginate is considered a nonbiodegradable biomaterial (31). However, covalently linked gels can be disassembled by swelling and ion-exchange reactions and dependent on the molecular weight might be eliminated from the body via macrophage uptake in the spleen or renal excretion (32).

Due to the poor cell-alginate interactions, alginates can be combined with other biopolymers such as Matrigel, collagen and fibrin to facilitate cell adhesion (10). Alginate itself can also be modified to facilitate cell adhesion. By sulfation of the free hydroxyl groups on the alginates can they show similar properties to the GAGs found in the ECM (33) or be functionalized by the addition of synthetic RGD peptides (8). While viscosity and modifications can be altered by using functionalized alginates with high molecular weight and G content, it lacks structural fidelity to maintain their intended structure prior to crosslinking. Therefore, alginate hydrogels can be combined with other biocompatible materials that have higher structural fidelity, such as cellulose (19).

1.3.3 Cellulose

Cellulose is the primary component of plant and green algal cell walls, and it is also produced by fungus and bacteria. Tunicates, a group of primitive sea invertebrates, are the only animals that produce cellulose. Cellulose is the most abundant naturally occurring polysaccharide (34) and has a simple chemical structure. It is a linear polymer with only one monomer, the β-D-glucose, connected between carbon 1 and carbon 4. It has a high degree of crystallinity, which results in strong chain-to-chain interactions and makes it very resistant to degradation. Nano fibrillated cellulose (NFC) are nanosized cellulose fibrils (25). NFC derived from tunicates have a naturally high degree of crystallinity and can be produced without contamination of lignin and hemicellulose (35). Cellulose can also be TEMPO-oxidized to convert cellulose fibres into NFC. This is done by the introduction of sodium carboxyl groups on the surfaces of cellulose elementary fibrils (36). NFC has a high aspect ratio with a lateral dimension of 5-20 nanometres and a longitudinal dimension of up to several micrometres (25). It is used as a reinforcing

material with other hydrogels since it is biocompatible, biodegradable and has a broad capacity for chemical modifications (19).

1.4 Rheology

Rheology, the science of material deformation, can be used to predict the mechanical properties of hydrogels (37). One of these properties is viscosity, which is defined as a material's resistance to flow. The viscosity is determined by the polymer concentration and molecular weight (6) and is an important parameter in 3D-bioprinting because it contributes to shape maintenance and structural fidelity. The viscosity also indicates whether the bioink will flow during extrusion, which is known as shear-thinning behaviour (37). The viscosity of a sample is determined by applying a force to it and measuring the displacement gradient over time (38). This continuous shear measurement can generate a flow curve with shear viscosity (Pa) versus shear rate (s^{-1}) which indicates whether or not the bioink sample is shear-thinning (39).

The storage modulus (G') and loss modulus (G'') of a bioink represent the elastic and viscous components, respectively, and increase with increasing solid-like or viscous-like behaviour of the sample in question (40). Amplitude sweeps are used to determine the linear viscoelastic region (LVR) of a bioink where G' and G'' are not affected by the applied stress and strain. Oscillatory frequency sweeps are performed within the LVR to analyse the viscoelastic responses at a wide range of loading frequencies. This measurement can give an insight into the polymer structures and whether the material is a viscoelastic solid or a viscoelastic liquid. As the gel state is characterized by the dominance of elastic behaviour over viscous behaviour, viscoelastic solid-like hydrogels are generally more desired as bioinks (39). The ratio between G' and G'' is estimated by the phase angle (δ) which indicates whether the material is primarily viscous $\delta > 45°$ (G' < G'') or elastic $\delta < 45°$ (G' > G''). During a measurement where the bioink is crosslinked, the solid to gel transition can be estimated for $\delta = 45°$ (G'= G'') (40).

1.5 Alginate and NFC-based bioinks

In three previous works, Markstedt et al. (19), Müller et al. (24), and Im et al. (41) investigated bioinks composed of alginate and nano fibrillated cellulose (NFC) for 3D-bioprinting and 3D cell cultivation. In all three studies, the formulated bioinks were mixed with chondrocyte or osteoblast cells and subsequently printed. Different compositions and ratios of alginate and NFC were investigated and bioinks that showed great printability, as well as rheological

properties suited for 3D-bioprinting, were subsequently investigated. The papers established that alginate and NFC-based bioinks have rheological properties suitable for 3D-bioprinting.

Markstedt et al. used sterile unmodified alginates mixed with NFC without the addition of any growth-enhancing proteins and still achieved a high chondrocyte cell viability of more than 70%. In Müller et al., the bioinks were optimized for biological activity by the addition of sulfated alginates while in Im et al. were polydopamine nanoparticles (PDANP) incorporated. With the addition of sulfated alginates with NFC did chondrocyte cells show significant proliferation and increase in cell numbers compared to non-sulfated alginate-NFC bioinks. The incorporation of PDANP resulted in higher metabolic activity of osteoblast cells, most likely due to the PDNAPs absorption of nutrients from the medium (41). Cell proliferation and viability of cells can thus be increased by incorporating additives that support the growth of cells. Cytotoxicity, metabolic activity, and immunohistochemistry tests of the encapsulated cells indicated that all formulated bioinks were biocompatible and the cells demonstrated high viability after printing, ranging from 70% right after crosslinking (19) to 88% after 28 days of cultivation (24).

1.6 Research concept

The main objective of this master's thesis was to develop and characterize novel bioinks of functionalized alginates for use in 3D-bioprinting. Because unmodified alginates are inert toward cells and do not promote adhesion and tissue formation, RGD functionalized alginates were mixed with unmodified alginates. Alginates alone lack the structural integrity to retain their intended structure after bioprinting. As a result, nano fibrillated cellulose from tunicates (TTC) was mixed with the alginates to create bioinks with the gelling properties of alginate and the structural properties of TTC. Bioinks composed of various TTC-alginate ratios, and different alginate structures, were characterized and selected based on printability, mechanical properties, and NHDF cell adhesion characteristics using rheology and visual observations. The master's thesis is structured into two main parts: biomaterial characterization and cell interactions, which are brought together via 3D-bioprinting. The main elements that were investigated are presented in Figure 5.

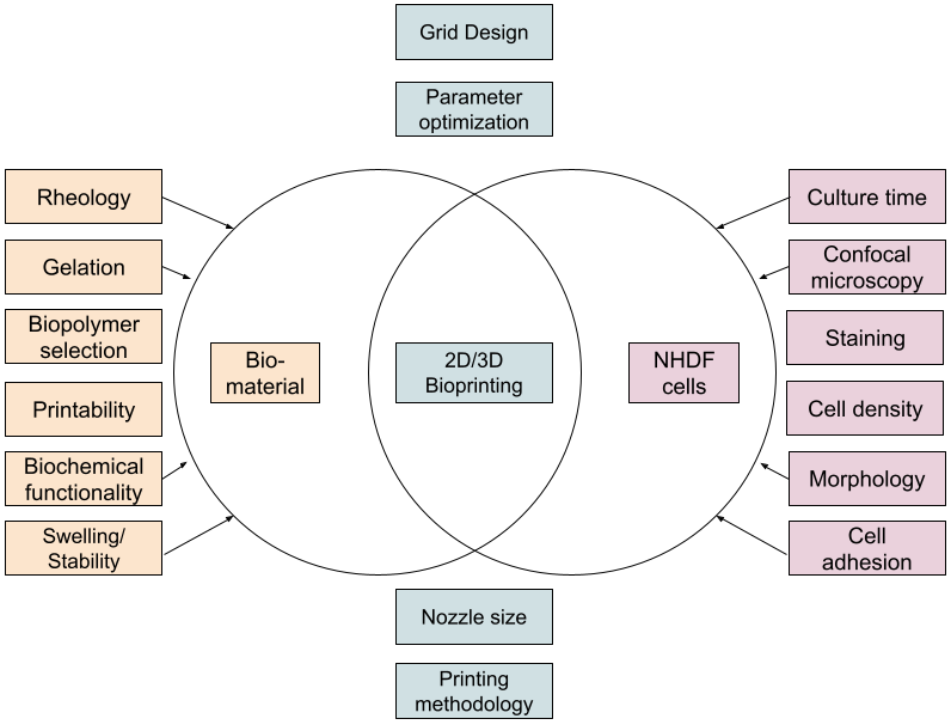

Figure 5 Overview of elements investigated in this master's thesis.

Cell-biomaterial interaction studies illustrated in Figure 6 were conducted with the bioinks that were best suited for 3D-bioprinting. The bioinks were assessed in these studies based on their ability to promote tissue formation and cell viability, using cell staining and confocal laser scanning microscopy (CLSM). Short-term incubations were performed to observe the initial

adhesion of the NHDF cells. After evaluation of the best suited bioink, an experiment with a long-term incubation period was performed to determine whether the bioink supported long-term cell growth.

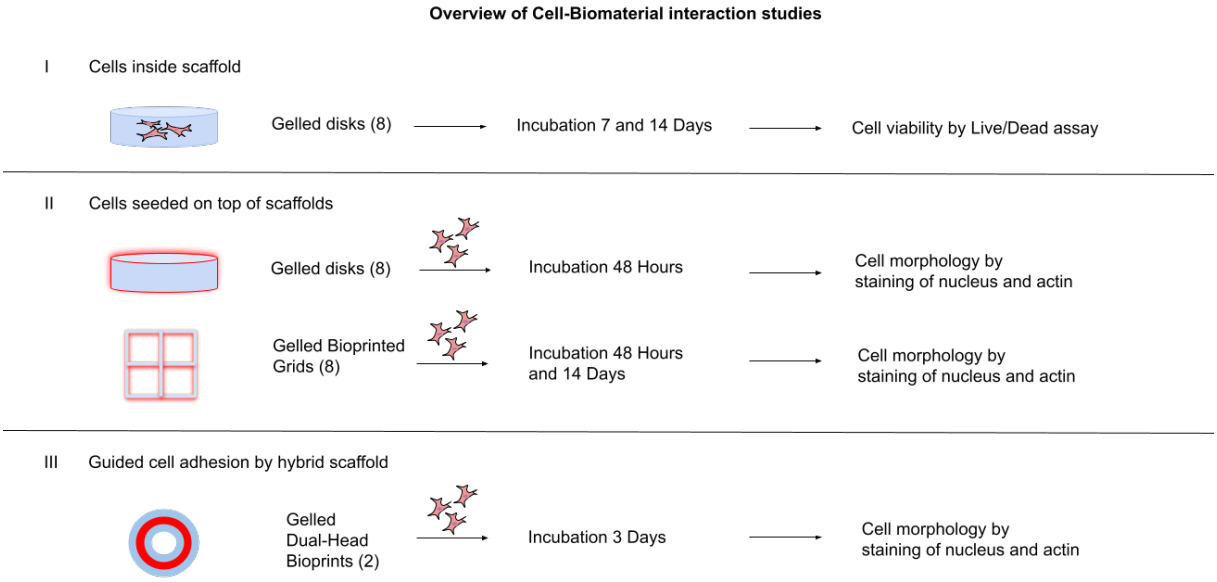

Figure 6 Overview of the cell-biomaterial interactions studies conducted throughout this thesis. Number in brackets indicates the number of different bioinks used in the experiments.

In order to answer the main objective, this thesis will seek to answer the following research questions:

- How do the molecular weight, G-content and concentration of alginates affect their properties regarding bioink formulation and printability in 3D-bioprinting?
- How does the rheological properties of TTC-alginate ratios affect the printability, stability, and gelation of formulated bioinks?
- Which composition of the formulated bioinks is best suited with regards to adhesion and compatibility with NHDF cells?
- How can 3D-bioprinting be used as a technique to guide cell attachment?

2. Materials and methods

2.1 Biomaterials

Throughout the experimental work presented in this thesis, six different alginates have been used. High molecular weight and low molecular weight alginates extracted from *Laminaria hyperborea* stipe were provided by Dupont Health & Nutrition (Norway). Low and high molecular weight alginates derived from *Pseudomonas fluorescence* mutants were produced and epimerized at SINTEF (Norway). Ultra-pure low viscosity sodium alginate with high guluronic acid (UPLVG) and 8% oxidation, and UPLVG with 8% oxidation and 5% substitution of GRGDSP, were produced by Dr. Aman S. Chahal based on alginates from NovaMatrix (Norway). Table 1 provides an overview of the alginates and their chemical specifications.

Table 1 Overview of alginates used with labels, source of origin, molecular weight in kDa and G-content in percent.

Label	Source	M_W (kDa)	G-content (%)
LHS-3	*Laminaria hyperborea* stipe	310	65-70
LHS-9	*Laminaria hyperborea* stipe	220	65-70
Pro22	*Pseudomonas fluorescence*	360	89
750PolyG	*Pseudomonas fluorescence*	184	85
Oxidized alginate	*Laminaria hyperborea* stipe	183	68
RGD-coupled alginate	*Laminaria hyperborea* stipe	182	68

2.1.1 Preparation of stock alginate solutions

For biomaterial characterizations, LHS-3, LHS-9, Pro22 and 750PolyG were dissolved in Milli-Q water with a magnetic stirrer at concentrations of 1.0%, 2.0% and 3.0% based on weight per volume ratio (w/v). For cell experiments, carbon filtered LHS-3 and Pro22 were dissolved in DMEM with additives at 3% (w/v).

2.1.2 Preparation of bioinks

Bioinks were generated by mixing stock solutions of alginates at 3% (w/v) with nano fibrillated cellulose (NFC) at different ratios. For biomaterial characterizations, 2.5% TEMPO-oxidized laboratory grade NFC derived from tunicates (TTC) (Ocean TuniCell, Norway) was used. For cell experiments, 2.5% TEMPO-oxidized medical grade TTC with 4.6% D-mannitol (TTC+M) (Ocean TuniCell, Norway) was used with dissolved carbon filtered alginates (see section 00). Bioinks used for cell experiments were mixed under sterile conditions. Female/female Luer locks (Cellink, USA) were used to transfer mixed bioinks from syringes to cartridges for bioprinting. Table 2 provides an overview of the generated bioinks as well as their compositions and the experiments in which they were used.

Table 2 Overview of the formulated bioinks used in the different experiments. Alginates were dissolved at 3% (w/v) and mixed with different ratios of TTC or TTC+M. Final alginate concentration of the bioinks was calculated in percent (%) and the bioinks is labeled to distinguish them. The bioinks used in the different experiments are marked with X.

Label	Dissolved alginates 3% (w/v)	TTC or TTC+M Ratios (Parts per 100)	Final alginate concentration (% w/v)	Experiments			
				Rheological measurements		Stability tests	Cell experiments
				Oscillation and Viscosity	Gelation		
Pro22-*6040*	Pro22	60	1.2	X		X	
Pro22-*7030*	Pro22	70	0.9	X		X	
Pro22-*8020*	Pro22	80	0.6	X		X	
LHS-3-*6040*	LHS-3	60	1.2	X		X	
LHS-3-*7030*	LHS-3	70	0.9	X		X	
LHS-3-*8020*	LHS-3	80	0.6	X		X	
Pro22-*7030*Ox	Pro22 0.75% UPLVG 2.25%	70	0.9		X	X	X
Pro22-*8020*Ox	Pro22 0.75% UPLVG 2.25%	80	0.6		X	X	X
LHS-3-*7030*Ox	LHS-3 0.75% UPLVG 2.25%	70	0.9		X	X	X
LHS-3-*8020*Ox	LHS-3 0.75% UPLVG 2.25%	80	0.6		X	X	X
Pro22-*7030RGD*	Pro22 0.75% GRGDSP 2.25%	70	0.9				X
Pro22-*8020RGD*	Pro22 0.75% GRGDSP 2.25%	80	0.6				X
LHS-3-*7030RGD*	LHS-3 0.75% GRGDSP 2.25%	70	0.9				X
LHS-3-*8020RGD*	LHS-3 0.75% GRGDSP 2.25%	80	0.6				X

2.2 Rheological measurements

A Kinexus Lab+ rheometer (Netzsch, Germany) was used for all rheological measurements. Raw data from rSpace (Netzsch, Germany) were collected and processed in Excel and GraphPad Prism.

2.2.1 Shear viscosity measurements of alginate concentrations

Shear viscosity was measured for each alginate concentration described in 2.1.1 using coaxial cylinders as inserted equipment; a DG25 bob, and a DO25 cup with a DI25 bottom (Netzsch, Germany). The cup was filled with approximately 5.4 ml of sample and the temperature was set to 37°C. The rSpace (Netzsch, Germany) Viscometry shear rate table was run with the start shear rate set to 0.1 s^{-1} and the end shear rate set to 10.0 s^{-1}. Ten samples were taken per decade with logarithmic progression.

2.2.2 Oscillation and viscosity measurements of bioinks

Bioinks described in Table 2 under Oscillation and Viscosity were prepared for measurements as stated in section 2.1.2. The sequence consisted of amplitude sweep strain and stress controls, and frequency sweep strain and stress controls. The linear viscoelastic region (LVR) and optimal strain of the bioinks was determined using amplitude sweeps. Frequency stress and strain controls were used to record the viscoelastic spectrum of the bioinks.

For all measurements, CP1/40 cone (Netzsch, Germany) with 1° angle and 40 mm diameter and a PLS40 plate (Netzsch, Germany) with 40 mm diameter were used. Approximately 1 ml of sample was loaded on the plate and the cone was descended to a gap at 0.028 mm. After the gap was set, the samples were trimmed with Q-tips. Before measurement was each sample equilibrated to measuring temperature at 25°C. Amplitude strain and stress controls were performed with a start shear strain of 0.1 %, an end shear strain of 10^3 %, and a set frequency of 1 Hz, with ten samples taken per decade using logarithmic progression.

For each sample were optimal strain from amplitude strain control used as strain in the frequency strain and stress controls. Start frequency was set to 100 Hz and end frequency was set to 0.001 Hz. When harmonic distortion (HD) became non-linear, the sequence was terminated. Ten samples were taken per decade with logarithmic progression.

Shear viscosity measurements of the six bioinks were performed on the same samples as in the amplitude and frequency sweeps. The rSpace (Netzsch, Germany) Viscometry shear rate table was run with the start shear rate set to 10^{-3} s^{-1} and the end shear rate set to 10^{4} s^{-1}. Ten samples were taken per decade with logarithmic progression.

2.2.3 Gelation measurements of bioinks with oxidised alginate

Bioinks described in Table 2 under Gelation, were prepared for measurements as stated in 2.1.2. The sequence was utilized in rSpace and consisted of a viscometry ramp, oscillation frequency table and oscillation single frequency measurements before and after the addition of 0.1 M $CaCl_2$. The 0.1 M $CaCl_2$ was pipetted around the loaded samples for the diffusion of Ca^{2+} ions.

A CP1/20 cone (Netzsch, Germany) with 1° angle and 20 mm diameter and a PLS60 plate (Netzsch, Germany) with 60 mm diameter were used. Approximately 0.5 mL of sample was loaded, and the cone was descended into a defined gap of 1.1 mm. The samples were trimmed with Q-tips. The viscometry ramp began with a shear rate of 0.1 s^{-1}, increased to 100 s^{-1}, and then returned to 0.1 s^{-1} while ten samples were taken per decade with logarithmic progression. Oscillation frequency tables before and after gelation had the following parameters: start frequency at 10 Hz, end frequency at 0.1 Hz, shear strain 0.1 %, and a logarithmic progression of 10 samples per decade.

The change in storage modulus (G'), loss modulus (G''), and phase angle (δ) were evaluated using oscillation with single frequency at 1.0 Hz and shear strain at 0.1 %. Twenty samples were taken prior to gelation. After adding 0.1 M $CaCl_2$, the sample was oscillated with the same frequency and shear strain over a course of 60 minutes, yielding 720 measurements.

2.3 Carbon filtration of Pro22 and LHS-3

High molecular weight bacterial alginate Pro22, and stipe alginate LHS-3 were purified by powdered carbon filtration. Pro22 and LHS-3 were dissolved with MilliQ Water to a concentration of 2 mg/ml and 4 mg/ml. Bentonorit CA1 activated carbon (Cabot, USA) was added to the alginate solutions with a ratio of 10 grams per 1 gram of alginate. To neutralize the solutions was 2M NaOH added. The solutions were incubated in a shaking incubator at 45°C with 100 RPM overnight.

Whatman filter papers (Cytiva, Great Britain) with 11 μm pore size were placed in a Büchner funnel and the filters were precoated with IFAB Filter Aid (Skandinaviska IFAB Filtering AB, Sweden) where 0.9 g/cm of dissolved diatom De 30 and diatom De100 were added. A body feed concentration of 7% (both De 30 and De 100) was blended into both alginate solutions. The filtered solutions were added 3M NaOH until they reached a molar concentration of 0.1 M NaOH and were incubated in a water bath at 50°C for 45 minutes. After incubation were the solutions neutralized with 3M HCl. Carbon was added with a ratio of 3 grams per gram of alginate and 3M NaOH was used to neutralize the solutions. The solutions were incubated in a shaking incubator at 45°C with 100 RPM overnight.

Filter papers were precoated with 0.7 g/cm of dissolved De 30 and De 100. A body feed concentration of approximately 1% was added of De 30 and De 100 to the solutions. After carbon filtration were the solutions sterile filtered through Nalgene Rapid-Flow sterile single use vacuum filters (Thermo Fisher Scientific, USA). The alginates were precipitated by adding 3M HCl and centrifuged at 7000 RPM for 15 minutes at room temperature. The supernatants were discarded, and the alginate pellets were cleansed with 0,05 M HCl and again centrifuged at 7000 RPM for 10 minutes. The alginate pellets were transferred to beakers with sterile water and dissolved by addition of 3 M NaOH. Dissolved alginate solutions were freeze-dried.

2.4 Stability and swelling tests of 3D-bioprinted scaffolds

All 3D-bioprinting experiments were carried out using the 3DDiscovery platform (RegenHu, Switzerland) shown in Figure 7.

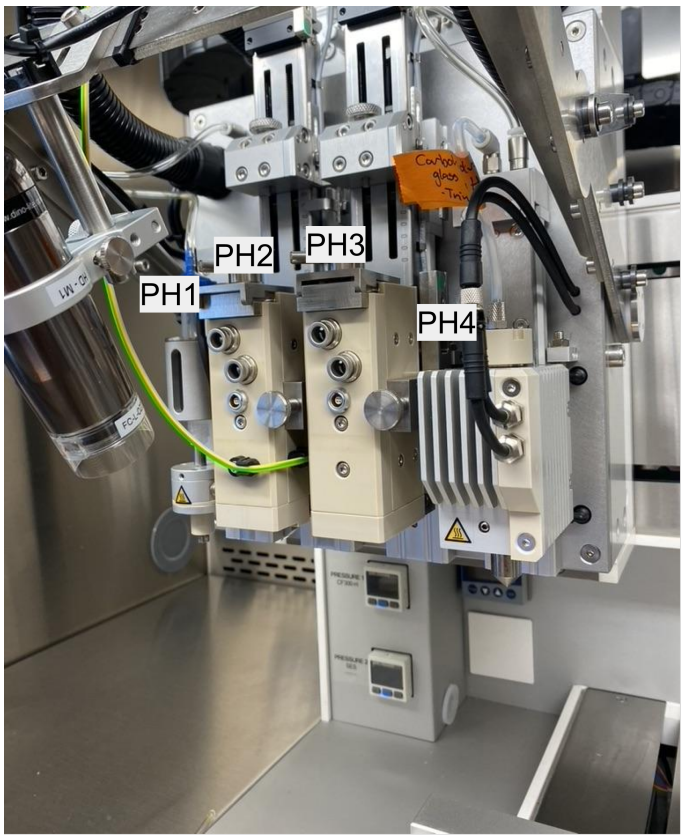

Figure 7 3DDiscovery bioprinter with four printheads based on different principles. PH1: inkjet printhead CF300H. PH2: Time-pressure based thermo polymer extruder. PH3: Extrusion based printhead by velocity control HPD-100 High-precision syringe pump dispenser PH4: Extrusion based printhead with air pressure DD-135H Time-pressure direct dispenser.

Bioinks described in Table 2 under Stability test were prepared and used in the 3D-bioprinting of grid scaffolds to determine their stability and swelling in physiological saline solution (PSS). Two sets of experiments were conducted. First with bioinks formulated with unmodified alginates and second with bioinks formulated with oxidized alginate.

A 12 x 12 mm grid was created in BioCAD™ (RegenHU, Switzerland) with horizontal and vertical filling tool path lines with 4 mm distance. The preview of the design is shown in Figure 8. The scaffolds were printed with a building count of 2 giving a predicted height of 0.64 mm.

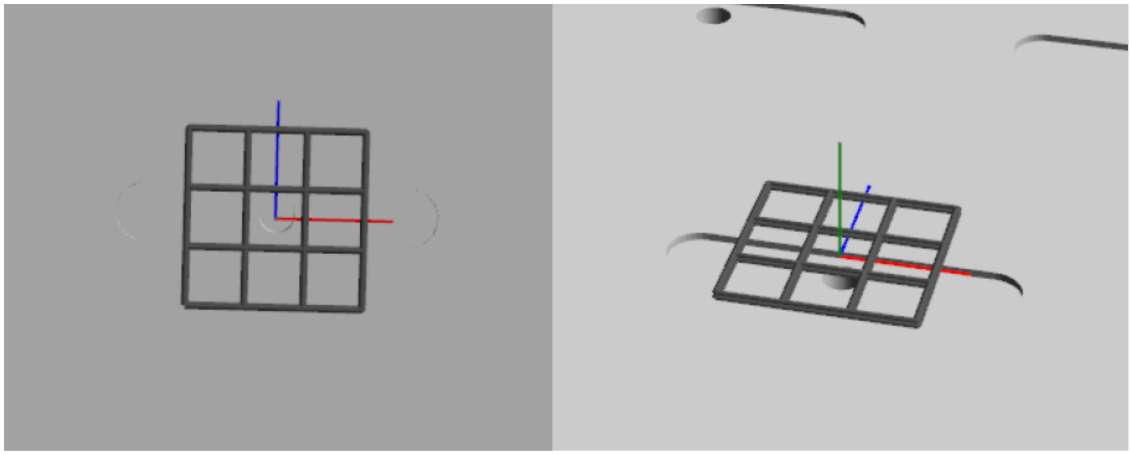

Figure 8 Scaffold created in BioCAD™ visualized in 3D Print Preview used for bioprinting bioinks for use in stability tests.

Table 3 shows the 3D-bioprinting parameters that were used in both experiments. The scaffolds were bioprinted with HPD-100 High-precision syringe pump dispenser (PH3) (RegenHu, Switzerland) in petri dishes, crosslinked with 0.1 M $CaCl_2$ and transferred to separate wells in a 12-well plate. The grids were imaged using a Leica S9i stereo microscope (Leica, Germany) at a magnification of 16x after printing, gelation, and over one week at 37°C incubation with daily replacement of a 0.154 M NaCl (PSS) medium.

Table 3 Bioprinting parameters for HPD-100 High-precision syringe pump dispenser (PH3) used in stability and swelling tests of bioinks composed of unmodified alginate mixed with TTC, and oxidized alginate mixed with carbon filtered alginates and TTC.

Parameters used for PH3	
Nozzle diameter	410 µm
Pressurize/Retract-distance	0.25 mm
Cartridge Diameter	7.290 mm
Volume Flow Rate	5.01 µl/s
Plunger Velocity	0.1200 mm/s
Material Thickness	0.320 mm
Feed Rate	15 mm/min
Strand Start Delay	200ns

2.5 Cell culture

2.5.1 NHDF cell cultivation and experiment preparation

Cell experiments were performed using adult Normal Human Dermal Fibroblasts (NHDF) from Lonza (Switzerland). Dulbecco's Modified Eagle Medium (DMEM) (Thermo Fisher Scientific, USA), with added 10% fetal bovine serum (FBS), 1 ng/mL fibroblast growth factor (FGF) and 10 mL/L penicillin and streptomycin was used for cultivation. Medium with added additives is referred to as DMEM+. The same medium was used for the maintenance, propagation and experimental purposes involving NHDF cells.

Cell cultures were split at 70-90% confluence by removing used medium and adding PBS (SINTEF Industry, Norway) for removal of medium residues before adding TrypLe express [+] phenol red (Gibco, USA) to detach the cells. TrypLe was inactivated after 2 minutes of incubation by adding DMEM+. The cell suspension was transferred to a tube and centrifuged at 1000 RPM at 25°C for 5 minutes. After removing the suspension, the cell pellet was resuspended in DMEM+ based on the wanted cell concentration. Cells were counted by mixing 10 µl of resuspended cells with 10 µl Trypan Blue (Thermo Fisher Scientific, USA) and transferring 10 µl of the mixture to a chamber slide. Loaded chamber slides were inserted into an automated cell counter, Countess II FL (Thermo Fisher Scientific, USA). A total of four replicas were counted, and the average was used as the cell number. The desired number of cells was then used in experiments and remaining cells were transferred to a new flask to continue cultivation. Cell cultures were maintained in a humidified incubator at 37°C and 5% CO_2 atmosphere.

2.5.2 Nucleus and cytoskeleton staining

Prior to staining the nucleus and cytoskeleton, cells were fixed and permeabilised using 4% formaldehyde and 1% Triton X-100 respectively. A staining buffer was prepared for dilution and washing purposes containing 10 mM HEPES buffer, 5 mM $CaCl_2$, and 0.14 M NaCl at pH 7.4. Prior to fixation and staining, samples were carefully washed. After one hour of incubation at room temperature, the fixation solution was removed, and the cells were washed twice.

The nucleus and cytoskeleton of the cells were stained with 1:1000 DAPI (Thermo Fisher Scientific, USA) and 1:400 Phalloidin Alexa Fluor (Thermo Fisher Scientific, USA). Two different phalloidins were used, one that excites at 488 nm and one at 568 nm. Cells were

washed twice with staining buffer after one hour of incubation at room temperature, and the cells were stored in staining buffer, protected from light at 4°C.

2.6 NHDF cells embedded in bioinks

2.6.1 7-Day incubation

Bioinks presented in Table 2 under Cell experiment column were prepared as described in 2.1.2. Approximately 200 µl of each bioink was transferred to 1 ml syringes (Henke-Ject, Germany). Cultivated NHDF cells at passage 11 were trypsinized as described in 2.5.1 and resuspended in 1 ml of DMEM+ to a cell concentration of 1.09 x 10^6 cells/ml. Cell-bioink mixtures were transferred back and forth between syringe and pipette until creation of a homogenous cell-bioink gel. Duplicates of 100 µl cell-bioink mixtures loaded with 3.5x10^4 cells, were deposited on disk casters (QGel SA, Switzerland) and transferred for approximately 4 minutes to a reagent reservoir (VWR, USA) containing filtrated $CaCl_2$. The disks were transferred to 24 well plates using autoclaved metal spatulas after gelation. DMEM+ was carefully added along the side of the wells until the disks were submerged. The disks were incubated for 7 days in a humidified incubator at 37°C and 5% CO_2 atmosphere. Media was changed every third day.

2.6.2 14-Day incubation

Bioinks presented in Table 2 under Cell experiments were prepared as described in 2.1.2. The cell-bioink mixture was made as described in 2.6.1 with the following modifications. Trypsinized cells at passage 14 were centrifuged and resuspended in 2 ml DMEM+, resulting in a reduced cell concentration of 3.32 x 10^5 cells/ml. Cell loaded bioink disks contained 2.5x10^4 cells. The Pro22*8020*Ox cell-bioink mixture dissolved when the disk caster was descended into 0.1M $CaCl_2$, due to the large volume of cell suspension. The rest of the disks were cultured for 14 days in a humidified incubator at 37°C and 5% CO_2 atmosphere, and media was changed every third day.

2.6.3 Live/Dead Assay

A staining solution composed of DMEM with 0.2% EthD-1 (Thermo Fisher Scientific, USA) and 0.05% Calcein-AM (Thermo Fisher Scientific, USA) was used to stain NHDF cells inside the disks. The disks were covered with the staining solution and incubated in a humidified incubator at 37°C and 5% CO_2 atmosphere for 75 minutes. Live/dead staining was conducted on day 7 and day 14.

2.7 Cells seeded on bioink disks

Bioinks mixed with RGD coupled alginate presented in Table 2 under Cell experiment were prepared as described in 2.1.2. Triplicates of 100 µl bioinks were deposited on disk casters (QGel SA, Switzerland) and submerged in sterile-filtered 0.1 M $CaCl_2$. The disks were transferred to separate wells in 24 well plates using autoclaved metal spatulas after gelation. Trypsinized passage 14 cells were seeded on top of the disks with a concentration of 4.6 x 10^4 cells per disk. After one hour of incubation, DMEM+ was carefully added along the side of the wells until the disks were covered. The disks were incubated in a humidified incubator at 37°C and 5% CO_2 atmosphere. After 24 hours, the disks were preserved and stained as described in 2.5.2 with Phalloidin 568.

The experiment was repeated with the following modifications. As controls, bioinks containing oxidized alginate were added. Passage 8 NHDF cells were used, with an optimized cell seeding density of 1.7 x 10^4 cells per disk. The incubation time of the cells were prolonged to 48 hours.

2.8 Cells seeded on 3D-bioprinted scaffolds

In BioCAD™ (RegenHU, Switzerland), a 6 x 6 mm grid was created with horizontal and vertical filling tool path lines at 3.0 mm. The scaffold was printed with a building count of two giving an estimated height of 0.70 mm. The preview of the design is shown in Figure 9.

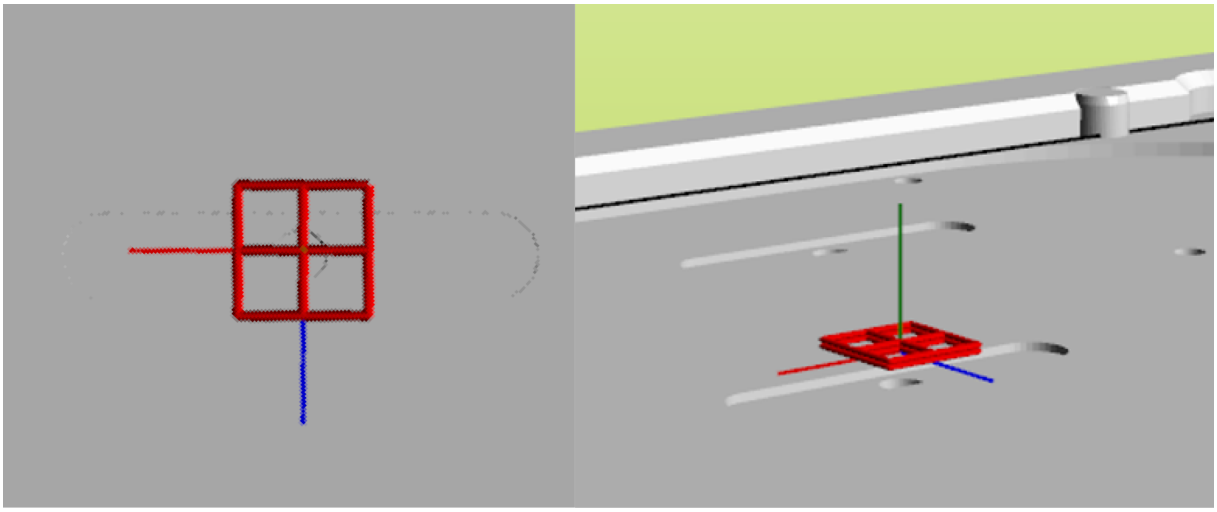

Figure 9 Scaffold designed in BioCAD™ for cell experiments. Visualized in 3D Print Preview.

The scaffolds were 3D-bioprinted using HPD-100 High-precision syringe pump dispenser (PH3) (RegenHu, Switzerland) and the parameters used are presented below in Table 4.

Table 4 Bioprinting parameters for HPD-100 High-precision syringe pump dispenser (PH3) used for printing of 6x6 mm scaffolds for cell experiment.

Parameters used for PH3	
Nozzle diameter	410 µm
Pressurize/Retract-distance	0.20 mm
Cartridge Diameter	7.290 mm
Volume Flow Rate	2.086 µl/s
Plunger Velocity	0.05 mm/s
Material Thickness	0.350 mm
Feed Rate	8 mm/min
Strand Start Delay	200 ns

2.8.1 Short-term culture

All eight bioinks presented in Table 2 under Cell experiment were prepared as described in 2.1.2. Bioinks were transferred to autoclaved gastight 2.5 ml cartridge (Hamilton, USA), between bioink changes were the cartridge cleansed with MilliQ water. Autoclaved 22G nozzles (Cellink, USA) were used and changed between each bioink. Duplicates of each scaffold were printed in petri dishes and covered with 0.1 M $CaCl_2$ for approximately 5 minutes before the $CaCl_2$ was removed, and the grids were placed in separate wells in a 24 well plate using autoclaved metal spatulas.

Passage 10 NHDF cells were prepared for the experiment as explained in 2.5.1. With a concentration of 2.21 x 10^4 per 30 µl were cell suspensions added on top of the scaffolds. The well plates were set in a humidified incubator at 37°C and 5% CO_2 atmosphere for 1 hour for cell attachment. After 1 hour were the scaffolds covered with DMEM+. The cells were preserved after a 48-hour incubation period, and the nuclei and cytoskeletons were stained with Phalloidin 568 and DAPI as described in section 2.5.2.

2.8.2 Long-term culture

The experiment was conducted as described in 2.8.1 with the following modifications. LHS-3-*7030*RGD bioink was prepared as described in 2.1.2. Passage 12 NHDF cells were prepared for the experiment as described in 2.5.1 with a concentration of 2.0 x 10^4 cells per 30 µl. The scaffolds were seeded with 30 µl cell suspension and cultured for 14 days in a humidified incubator at 37°C and 5% CO_2 atmosphere, with the media changed every third day. The cells were preserved after a 14-day incubation period, and the nucleus and cytoskeleton were stained with Phalloidin 488 and DAPI as described in section 2.5.2.

2.9 Cell guidance via controlled production of hybrid 3D-bioprinted materials

Figure 10 shows the spiral design created in BioCAD™ (RegenHU, Switzerland) for hybrid 3D-bioprinted materials. Red lines represent alginate materials functionalised with RGD peptide which were 3D-bioprinted with HPD-100 High-precision syringe pump dispenser (PH3), while black lines show the deposition of oxidised alginates which were 3D-bioprinted with DD-135H Time-pressure direct dispenser (PH4) (RegenHu).

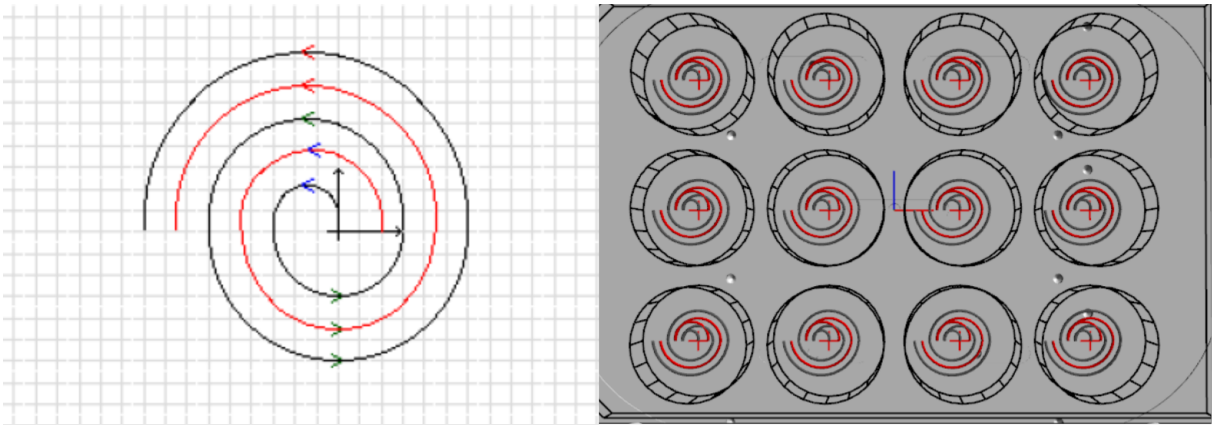

Figure 10 Spiral design for dual head bioprinting with PH3 (red lines) and PH4 (black lines). Left: design created in BioCAD™. Right: Design visualized in 3D print preview.

LHS-3-*7030*RGD and LHS-3-*7030*Ox presented in Table 2 under the Cell experiments column were prepared as described in 2.1.2. LHS-3-*7030*RGD were transferred to an autoclaved gastight 2.5 ml cartridge (Hamilton, USA) for bioprinting with HPD-100 High-precision syringe pump dispenser (PH3) (RegenHU, Switzerland). LHS-3-*7030*Ox was transferred to a sterilized 5CC cartridge with piston (RegenHU, Switzerland) for bioprinting with DD-135H Time-pressure direct dispenser (PH4) (RegenHU, Switzerland). Both printheads were installed with autoclaved 22G nozzles (Cellink, USA) with a nozzle diameter of 410 µm. Triplicates of

each scaffold were printed in 12-well plates and crosslinked with 0.1 M $CaCl_2$. The printing parameters used for PH3 and PH4 are presented below in Table 5.

Table 5 3D-bioprinting parameters used for HPD-100 High-precision syringe pump dispenser (PH3) and DD-135H Time-pressure direct dispenser (PH4) for dual head bioprinting.

Parameters used for:	PH3	PH4
Nozzle diameter (µm)	410	410
Pressurize/Retract-distance (mm)	0.15	-
Cartridge Diameter (mm)	7.290	-
Volume Flow Rate (µl/s)	2.09-2.29	-
Plunger Velocity (mm/s)	0.04-0.05	-
Material Thickness (mm)	0.350	0.350
Feed Rate (mm/min)	8	8
Strand Start Delay (ns)	100	100
Air Pressure (mPa)	-	0.01-0.015

Passage 15 NHDF cells were prepared for the experiment as described in 2.5.1. Cells were seeded with a concentration of 3.98 x 10^4 cells per spiral. The well plates were set in a humidified incubator at 37°C and 5% CO_2 atmosphere for 1 hour for cell attachment. After 1 hour were the scaffolds covered with DMEM+. After three days of incubation, the cells were preserved and stained as explained in section 2.5.2.

2.10 Confocal microscopy

Confocal laser scanning microscope (CLSM), Leica SP8 (Leica, Germany) was used to investigate cell viability, morphology and spreading. Z-stacks showed in the results section of this thesis range from 3.50 µm – 363 µm with a resolution of 1024 × 1024 pixels. DAPI was excited with a 405 nm laser while Phalloidin was excited with a 568 nm or 488 nm laser to capture stained nuclei and cytoskeletons. The disks and scaffolds were transferred to new wells upside down with plastic spatulas to avoid interference from cells at the bottom of the wells. Confocal images of the cells seeded on disks were taken with a 10x objective while images of the cells seeded on scaffolds were taken with a 5x objective, both with a dry lens. Tile scans were used to capture an overview of the cell distribution on the spiral scaffolds. The tile scans were processed directly in LasX, where they were merged into a single image and the maximum

composition of the z-stacks were processed. Fiji ImageJ was used to analyse and process all CLSM images.

2.10.1 Live/dead staining of NHDF cells mixed in bioinks

Confocal images of cells inside disks were captured with a 5x objective with a dry lens. In a sequential scan, Calcein-AM was excited with a 488 nm laser to capture live cells, while EthD-1 was excited with a 552 nm laser to capture dead cells. In Fiji ImageJ, z-stacks were composed to one maximum composition image and threshold were set to highlight all cells. After the threshold was set, the cells were counted using the Analyse particles plugin. Live and dead cells were counted separately. Dead cells accumulated in bubbles in some of the disks. As explained in Appendix C these were excluded from the count. Raw data from the ROI manager was exported to Excel for additional processing.

3. Results

3.1 Biomaterial characterization

3.1.1 Viscosity of alginate concentrations

Four different alginates at three different concentrations were prepared and studied to assess the effects of the structure and molecular weight on viscosity, and eligibility for bioink formulation. Figure 11 presents the viscosity flow curves for each sample. The high molecular weight alginates, LHS-3 (310 kDa) and Pro22 (360 kDa) demonstrated the highest viscosities. All concentrations of LHS-3, Pro22 and LHS-9 (220 kDa) demonstrated stable shear viscosities and were therefore not shear-thinning under the current experimental conditions. 750PolyG (184 kDa) showed an apparent shear-thinning at all three concentrations as the shear viscosity decreased as shear rate increased. A similar effect was observed for the lowest concentration of Pro22 and LHS-9, at low shear rates. Appendix A shows flow curves of LHS-7 (44 kDa), which were removed from further investigations due to its low viscosity, which made comparisons with the other alginate measurements difficult.

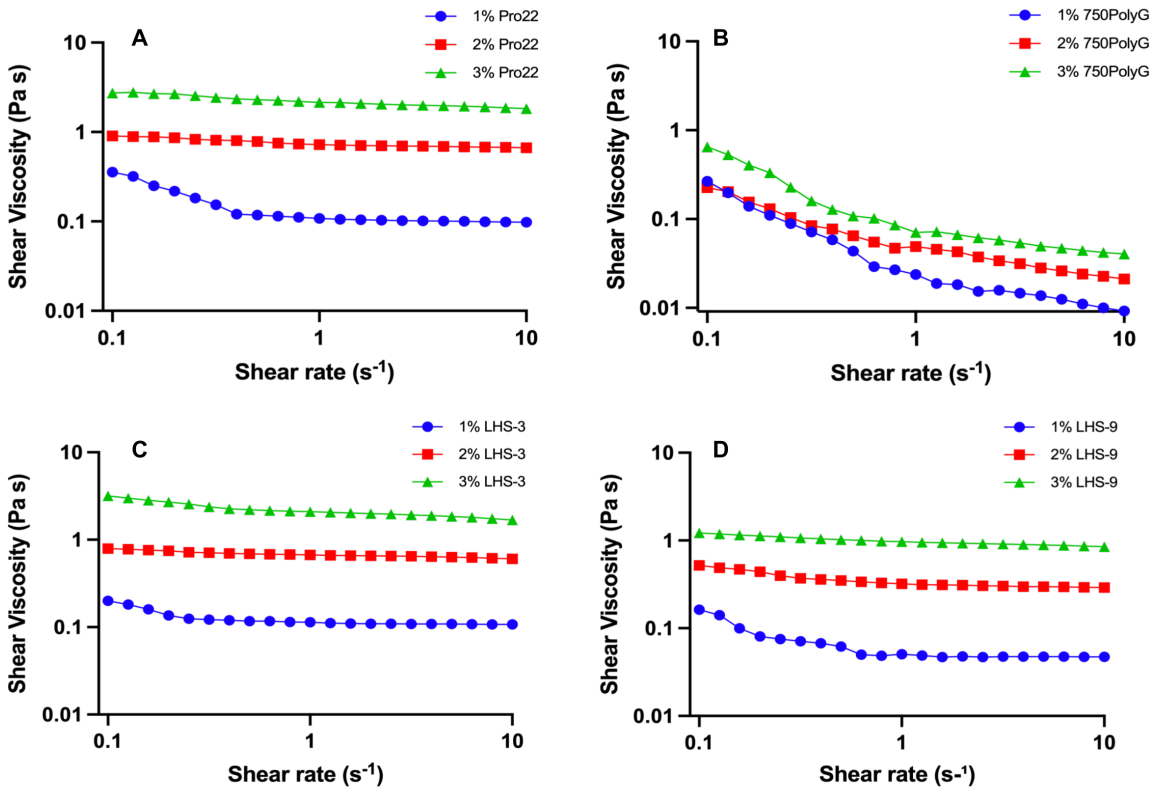

Figure 11 Flow curves of three alginate concentrations from each alginate sample. Shear viscosity (Pa s) was measured with shear rates from 0.1 s^{-1} to 10 s^{-1}. **A**: Viscosity flow curve of 1, 2 and 3% (w/v) Pro22 **B**: Viscosity flow curve of 1, 2 and 3% (w/v) 750PolyG **C**: Viscosity flow curve of 1, 2 and 3% (w/v) LHS-3 **D**: Viscosity flow curve of 1, 2 and 3% (w/v) LHS-9.

The flow curves of the highest alginate concentration of each alginate sample are shown in Figure 12. The flow curves of LHS-3 and Pro22 are almost identical and demonstrate the highest shear viscosities. The viscosity of LHS-9 was slightly lower than the two high molecular weight alginates while 750PolyG started at a viscosity close to LHS-9 but decreased sharply as shear rate increased. Based on comparably high and stable viscosities of Pro22 and LHS-3, these alginates were selected for subsequent studies.

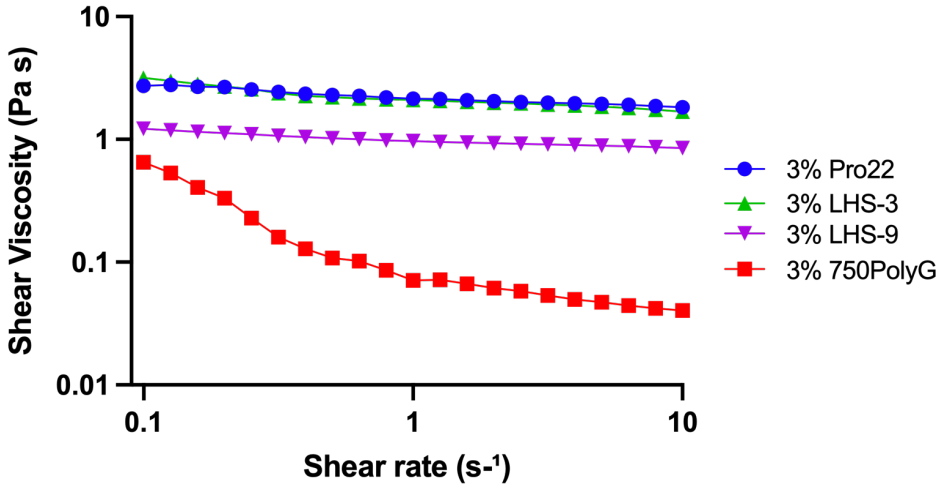

Figure 12 Comparison of the shear viscosity (Pa s) of the highest alginate concentrations from two bacterial alginates (Pro22 and 750PolyG) with low and high molecular weights and two kelp alginates (LHS-3 and LHS-9) with low and high molecular weights. Shear viscosity (Pa s) was measured with shear rates from 0.1 s^{-1} to 10 s^{-1}.

3.1.2 Viscosity of formulated bioinks

Figure 13 shows the flow curves of six different bioinks composed of LHS-3 and Pro22 mixed with TTC at three different ratios (TTC/alginate: 60/40, 70/30 and 80/20). Data points with steady-state measurements greater than 1.2 have been removed from the graphs due to poor signal-to-noise ratio. The different ratios were studied to find the most suitable proportions of alginate and TTC with regard to ease of extrusion and structural properties of the bioink. A pure TTC sample (2.5% w/v) was analysed as a control to see how the different alginate ratios influenced the rheological properties of the bioinks.

The shear viscosity of all six bioinks and the TTC sample was found to decrease sharply in response to an increasing shear rate, indicating good shear-thinning properties of the bioinks. TTC showed the highest shear viscosity flow curve in both graphs in Figure 13. In Figure 13 A, LHS-3-*7030* and LHS-3-*8020* show nearly identical flow curves while LHS-3-*6040* had the

lowest shear viscosity. The flow curves of the Pro22 70/30 and 80/20 ratios were closer to the TTC control than the LHS-3 samples.

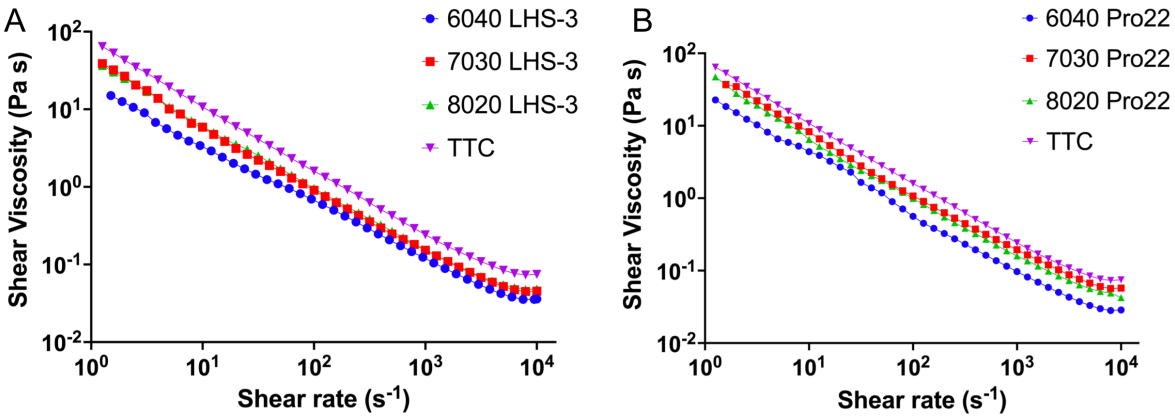

Figure 13 Flow curves of bioinks formulated of LHS-3 or Pro22 alginates at 3% (w/v) mixed with TTC at three different ratios (TTC/alginate 60/40, 70/30 or 80/20) as well as one pure TTC sample at 2.5% (w/v). Shear viscosity was measured with a shear rate range from 10^{-3} s^{-1} to 10^{4} s^{-1}. **A**: viscosity measurements of bioinks composed of LHS-3. **B**: viscosity measurements of bioinks composed of Pro22.

3.1.3 Frequency sweeps of formulated bioinks

Frequency sweeps were conducted to measure the viscoelastic spectrum of the bioinks and whether they showed gel behaviour or not. The optimal strain from each amplitude sweep test showed in Appendix B were used for the corresponding frequency sweep tests. The measurements were stopped when harmonic distortion went above 2%. Measurements above 39.81 Hz and below 1 Hz were excluded from the graphs due to high signal-to-noise ratios.

When the frequency was increased, storage modulus (G') and loss modulus (G'') for all bioinks in Figure 14 increased. For all six bioinks, G' was higher than G''. Higher TTC ratios resulted in higher G' measurements for the LHS-3 bioinks in Figure 14 A and the 70/30 ratio had the highest G'' measurements, followed by the 60/40 and 80/20 ratios, respectively. The 60/40 and 70/30 ratios of Pro22 bioinks in Figure 14 B demonstrated similar measurements for both G' and G'', where the 70/30 G' was slightly below 60/40 G'.

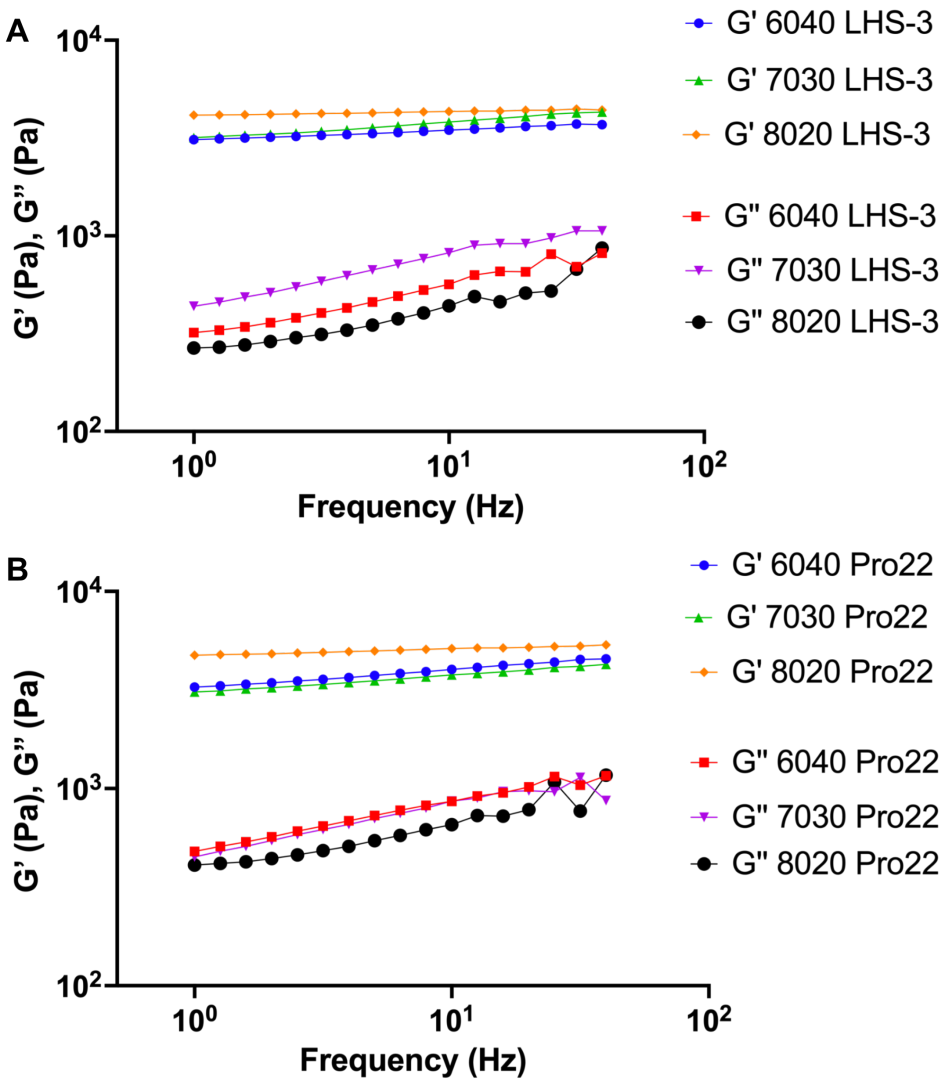

Figure 14 Frequency sweeps of bioinks formulated of LHS-3 or Pro22 mixed with TTC at three different ratios (TTC/alginate 60/40, 70/30 and 80/20). Storage modulus (G') and loss modulus (G'') was measured over a frequency range from 0.001 Hz to 100 Hz. Only measurements between 1.0 and 39.81 Hz are presented in the graphs due to high signal-to-noise ratios. **A**: Frequency sweeps of bioinks formulated with LHS-3. **B**: Frequency sweeps of bioinks formulated with Pro22.

3.1.4 Gelation of Pro22 and LHS-3 mixed with oxidised alginate and TTC

Oscillatory measurements were performed on LHS-3-*7030*Ox, LHS-3-*8020*Ox, Pro22-*7030*Ox, and Pro22-*8020*Ox during crosslinking with 0.1 M $CaCl_2$ to evaluate differences in gelation speed and final mechanical properties of the different alginate types and mixing ratios. Periodate oxidized alginates were included to simulate the contribution of peptide-coupled alginates. Figure 15 presents the change of storage modulus (G'), loss modulus (G'') and phase angle (δ) of the four bioinks over a 60-minute period.

G' and G'' of all four bioinks increased exponentially for approximately five minutes before turning into asymptotic increasing lines. In both graphs, G' and G'' was greater for the 70/30

ratios compared to the 80/20 ratios, and the Pro22 alginates showed higher G' and G'' values compared with LHS-3 for both mixing ratios. The difference between G' and G'' for the Pro22 ratios was smaller than the difference between G' and G'' for the LHS-3 ratios. As phase angles asymptotically decreased to less than 5°, similar mechanical structures were characterized for all four bioinks. Table 6 shows the measured G', G'' and δ after 60 minutes gelation of the four bioinks.

Table 6 Storage modulus (G') measured in Pascal (Pa), loss modulus (G'') measured in Pascal (Pa) and phase angle (δ) measured in degrees (°) of the four bioinks after 60-minutes of gelation with 0.1M $CaCl_2$.

	G' (Pa)	**G'' (Pa)**	**δ (°)**
LHS-3-*7030*Ox	2.40×10^4	2.10×10^3	4.82
LHS-3-*8020*Ox	1.67×10^4	1.34×10^3	4.57
Pro22-*7030*Ox	2.80×10^4	2.3×10^3	4.73
Pro22-*8020*Ox	2.41×10^4	1.97×10^3	4.68

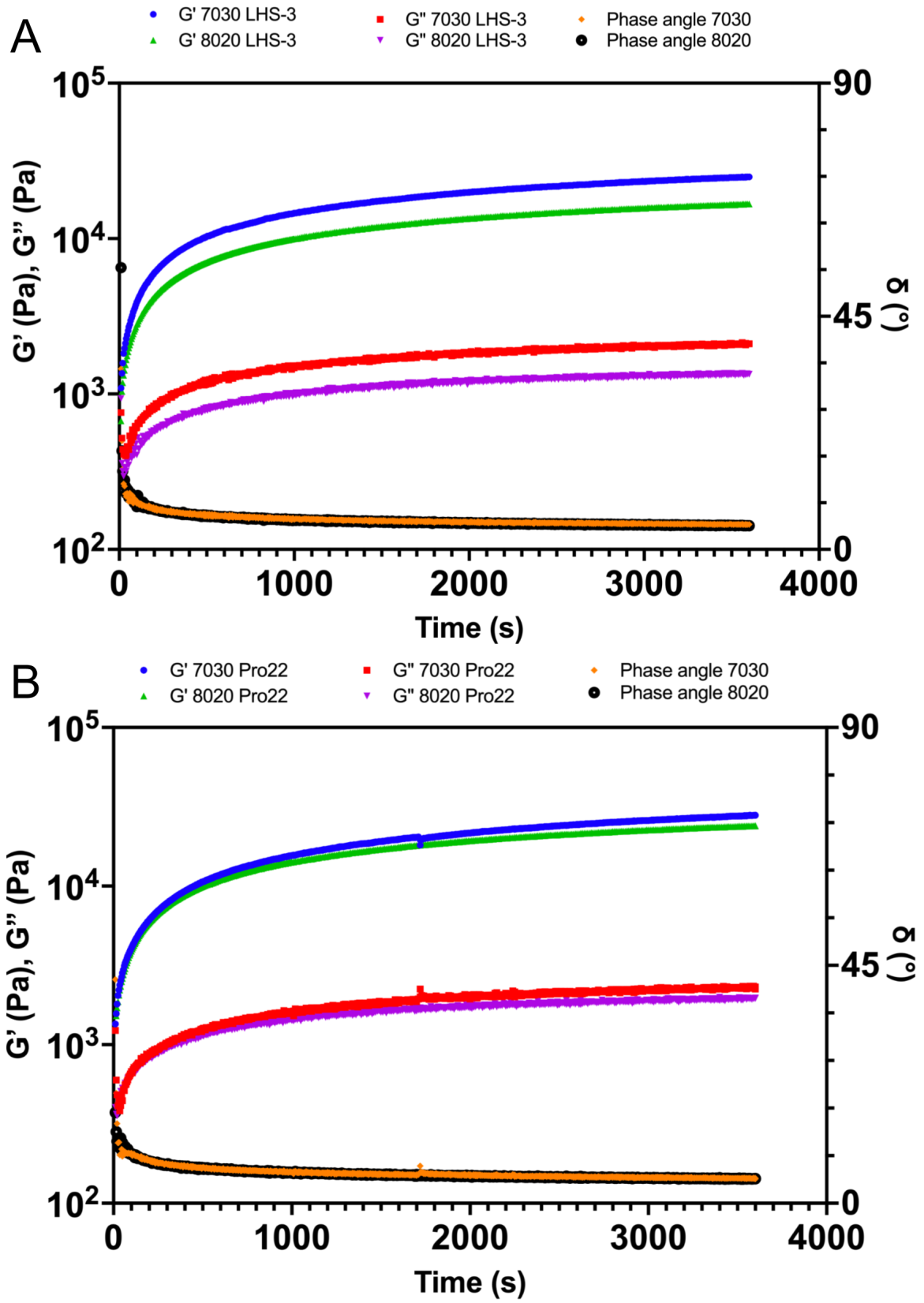

Figure 15 Gelation curves of bioinks composed of oxidized alginate (2.25% w/v) and Pro22 or LHS-3 (0.75% w/v) at two different TTC/alginate ratios (70/30 or 80/20). 0.1 M $CaCl_2$ were added around the samples during measurement to investigate gelation kinetics of the bioinks. Loss modulus (G'), storage modulus (G'') and phase angle (δ) were measured over a 60-minute period. **A**: Gelation curves of bioinks composed of LHS-3 and oxidized alginate. **B**: Gelation curves of bioinks composed of Pro22 and oxidized alginate.

3.2 Stability of bioprinted alginate-TTC scaffolds

3.2.1 Stability of scaffolds composed of unmodified alginates and TTC

The stability of six different 3D-bioprinted scaffolds composed of LHS-3 or Pro22 and TTC was examined in response to incubation in physiological saline solution (PSS) at 37°C, with a daily exchange of the medium. During the incubation period, the scaffolds were visually examined for any variations in their size, shape, or structural integrity. Figure 16 shows images of the scaffolds after they were printed, crosslinked, and incubated for 1 and 6 days.

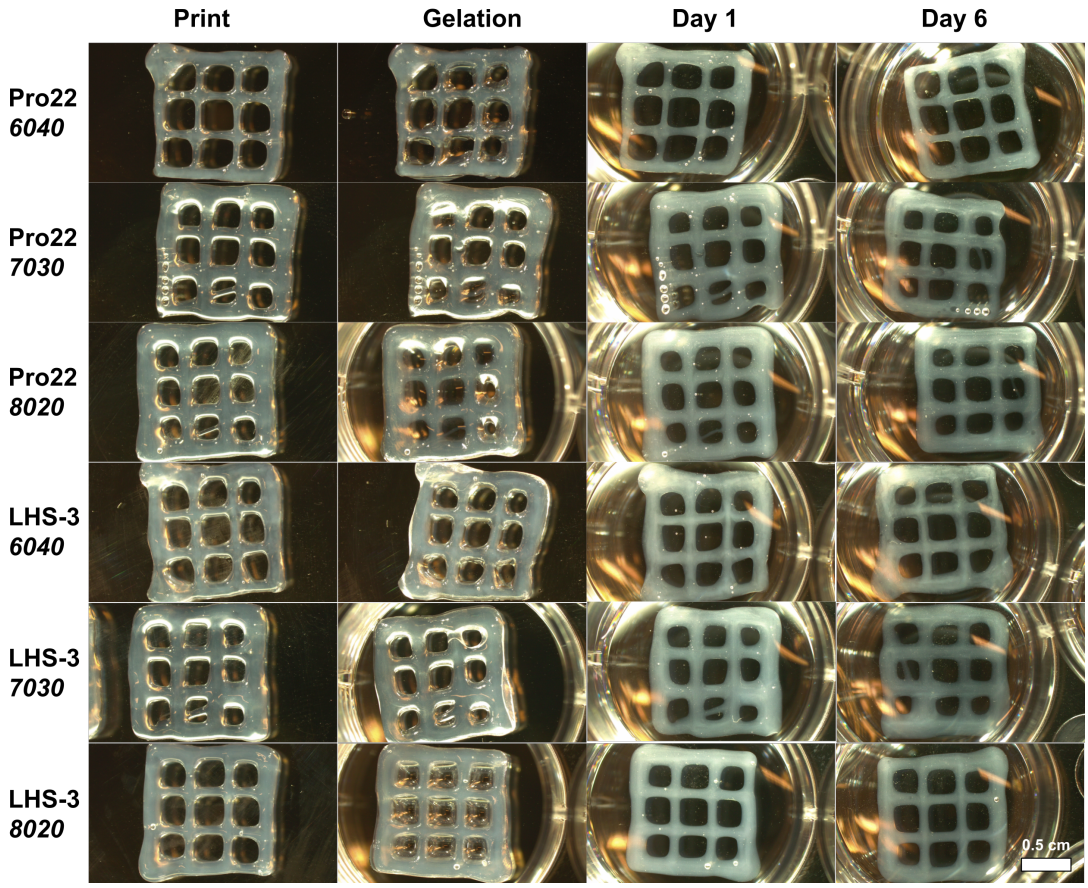

Figure 16 Pro22 and LHS-3 at 3% (v/w) concentration were mixed in three different ratios of TTC to generate six bioinks. The bioinks were bioprinted with the same scaffold design, crosslinked with 0.1M $CaCl_2$ and incubated in 0.154 M NaCl (PSS) at 37°C for six days. The NaCl were changed once each day of the incubation. The scaffolds were imaged after they were printed, crosslinked, 1 day of incubation and after 6 days of incubation. Scale bars correspond to 0.5 cm.

The structural integrity of all six scaffolds was preserved, with minor deformations due to the relocation from the printing bed to well plates. Some phase separation was observed in the 60/40 ratios for both alginate types, where the outer edges of the structures were more transparent than the inner parts. In the 70/30 and 80/20 ratios, this was less noticeable. Even though all six scaffolds appeared more see-through in Figure 16 on Day 6 compared to Day 1, this was presumably an optical effect from imaging the submerged scaffolds, as no significant

structural changes were observed over the incubation period upon visual inspection. Based on their apparent greater homogeneity and the higher measured shear viscosity (section 3.1.2), the 70/30 and 80/20 TTC/alginate ratios of each alginate type were selected for subsequent experiments.

3.2.2 Bioprinting and stability of bioinks with oxidized alginate

The stability of bioinks with oxidized alginate was evaluated similarly as described above in 3.2.1. The same scaffold design was used to bioprint the four bioinks composed of oxidized alginate dissolved with LHS-3 or Pro22 and mixed with two different TTC ratios (70/30 and 80/20). Figure 17 shows images of the scaffolds after they were printed, crosslinked, and incubated for 1 and 7 days.

The bioinks composed of oxidized alginate showed similar printability as the bioinks composed of unmodified alginates. The scaffolds were moved to separate wells in a well plate after gelation; throughout this procedure, the scaffolds were perceived to be more fragile than the unmodified scaffolds. Still, the structural integrity of the scaffolds was preserved and after 7 days of incubation, no significant structural changes of the scaffolds were observed.

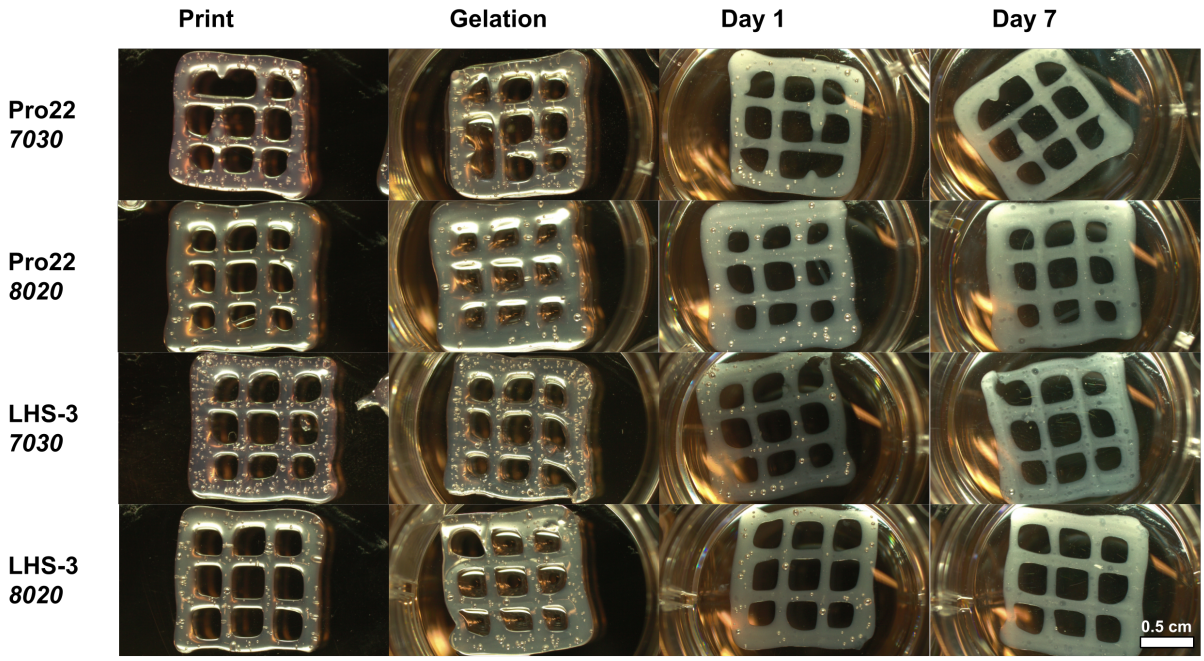

Figure 17 Pro22 and LHS-3 at 0.75% (w/v) were dissolved with 2.25% (w/v) oxidized alginate and mixed with two different ratios of TTC, generating four different bioinks. The bioinks were bioprinted with the same scaffold design and incubated in 0.154 M NaCl at 37°C for seven days. The NaCl were changed once each day of the incubation. The scaffolds were imaged after they were printed, crosslinked, 1 day of incubation and after 7 days of incubation. Scale bars correspond to 0.5 cm.

3.3 Live/dead assay and morphology of NHDF cells encapsulated in bioinks

NHDF cells mixed in crosslinked bioink disks were examined after 7 and 14 days to see if there were any differences in cell morphology and viability between the bioinks. The cells were stained with Live/Dead assay and imaged with CLSM for further processing and cell counting. Figure 18 and Figure 19 shows processed z-stack images of one representative replicate from each sample and cell viability (%) graphs for each time point.

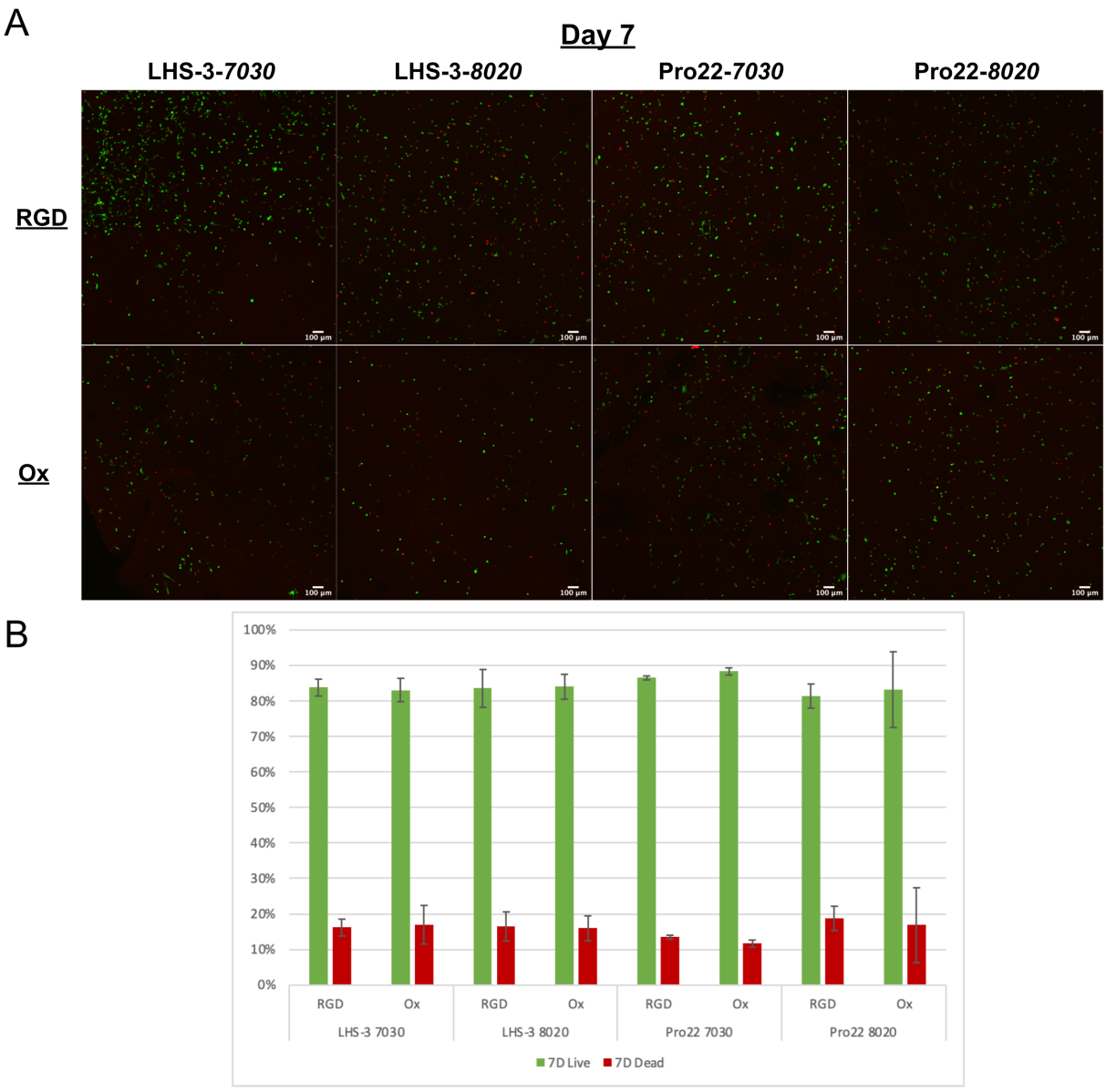

Figure 18 **A**: Live/Dead viability assay of NHDF cells encapsulated in bioinks after 7 days of incubation. Live cells were stained with Calcein AM (Green) and dead cells with EthD-1 (Red). Labels to the left refers to if the bioinks were RGD coupled (RGD) or negative controls with oxidized alginate (Ox). Labels on top refers to incubation period and the alginates (LHS-3 or Pro22) and ratios (70/30 or 80/20) used to formulate the bioinks. Scale bars correspond to 100 µm. **B**: Live and dead cell count (%) of NHDF cells mixed in crosslinked bioinks disks after 7-day incubation, represented as the average of individual duplicate counts ± standard deviation. Four of the bioinks were composed of RGD-coupled alginate, represented as RGD. Negative controls of the bioinks were included in the experiment, represented as Ox for oxidized alginate.

As seen in Figure 19 LHS-3-*7030*Ox, an air bubble was present where dead cells accumulated. These were excluded from the cell count as explained in Appendix C. The negative controls Pro22-*8020*Ox were not included in the 14-day incubation because they were dissolved during the crosslinking process.

At both timepoints, there were no noticeable differences in cell morphology between the RGD-based bioinks and the oxidized negative controls. While live/dead staining does not clearly highlight cell morphology, it indicates no significant differences in overall cell shape between the LHS-3 and Pro22 bioinks, nor between the 70/30 and 80/20 ratios. Majority of live cells in the images from Day 7 had rounded morphologies with some signs of protrusions, while a few cells were elongated. Many of the live cells in the Day 14 images were elongated, with several having a spindle-shaped morphology.

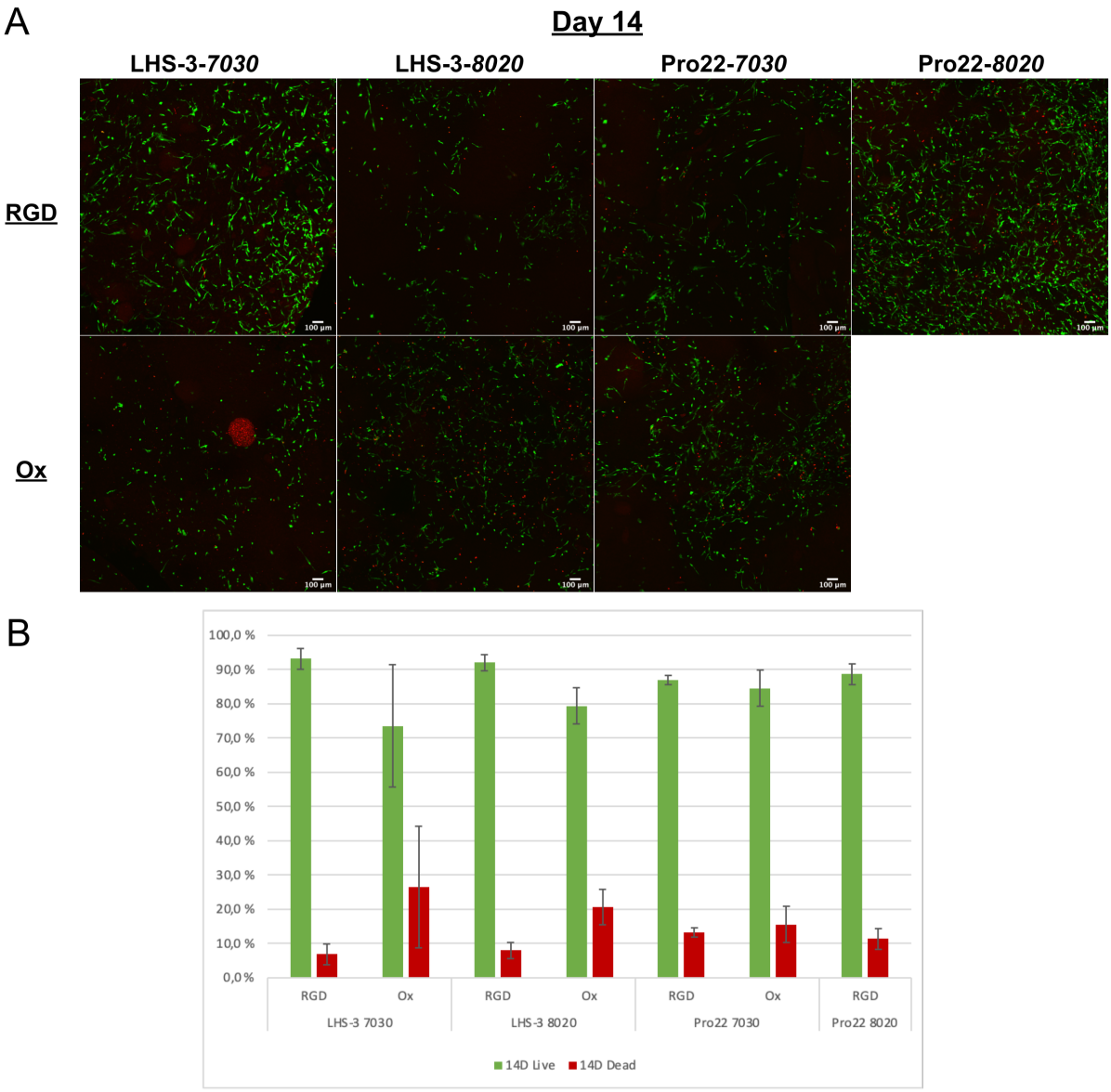

Figure 19 **A**: Live/Dead viability assay of NHDF cells encapsulated in bioinks after 14 days of incubation. Live cells were stained with Calcein AM (Green) and dead cells with EthD-1 (Red). Labels to the left refers to if the bioinks were RGD coupled (RGD) or negative controls with oxidized alginate (Ox). Labels on top refers to incubation period and the alginates (LHS-3 or Pro22) and ratios (70/30 or 80/20) used to formulate the bioinks. The Pro22-*8020*Ox duplicates were dissolved during the crosslinking process. Scale bars correspond to 100 µm. **B**: Live and dead cell count (%) of NHDF cells mixed in crosslinked bioinks disks after 14-day incubation, represented as the average of individual duplicate counts ± standard deviation. Four of the bioinks were composed of RGD-coupled alginate, represented as RGD. Negative controls of the bioinks were included in the experiment, represented as Ox for oxidized alginate.

3.4 Initial evaluation of cell adhesion on hydrogel disks

An initial experiment was conducted to evaluate if the RGD was functional in the mixtures of LHS-3 or Pro22 with TTC+M at 70/30 and 80/20 ratios (TTC+M/alginate). CLSM was used to examine the morphology and spreading of NHDF cells seeded on gel disks. Due to the low transparency of the bioinks, the gel disks were gently flipped upside down prior to imaging. Z-stacks were generated due to uneven topography resulting in cells on different vertical planes. The processed CLSM images from the initial 24-hour experiment are shown in Appendix 0.

To confirm our observations from the initial screening, an experiment with an optimised cell number, increased incubation period (48 h), and the inclusion of negative controls was performed. The processed CLSM images from the short-term experiment are presented in Figure 20. Cell interactions with bioinks formulated with RGD coupled alginate differed significantly from interactions with negative controls. As seen in Figure 20, cells seeded on negative controls were significantly fewer, irrespective of the alginate and TTC+M ratios. In fact, finding areas across the gel surface where cells had adhered to the control gels were problematic. The surface areas with the greatest number of cells were captured. All images of cells seeded on top of RGD formulated bioink disks showed that the cells had an elongated and spindle-shaped morphology, indicating that the cells had adhered and spread across the surface of all four bioinks.

Additionally, differences in cell behavior were observed across the negative controls with oxidized alginate. The negative control LHS-3-*7030*Ox showed a few elongated cells that had adhered to the bioink surface and to neighboring cells. Many of the cells had a rounded morphology with signs of protrusions. In LHS-3-*8020*Ox, the cytoskeleton staining was more visible as the cells had clustered. They had a spindle-shaped morphology without elongation, resulting in dense groups of cells. Cells seeded on Pro22-*7030*Ox had both elongated and round cells while the cells on Pro22-*8020*Ox were rounded or aggregated into one cell cluster.

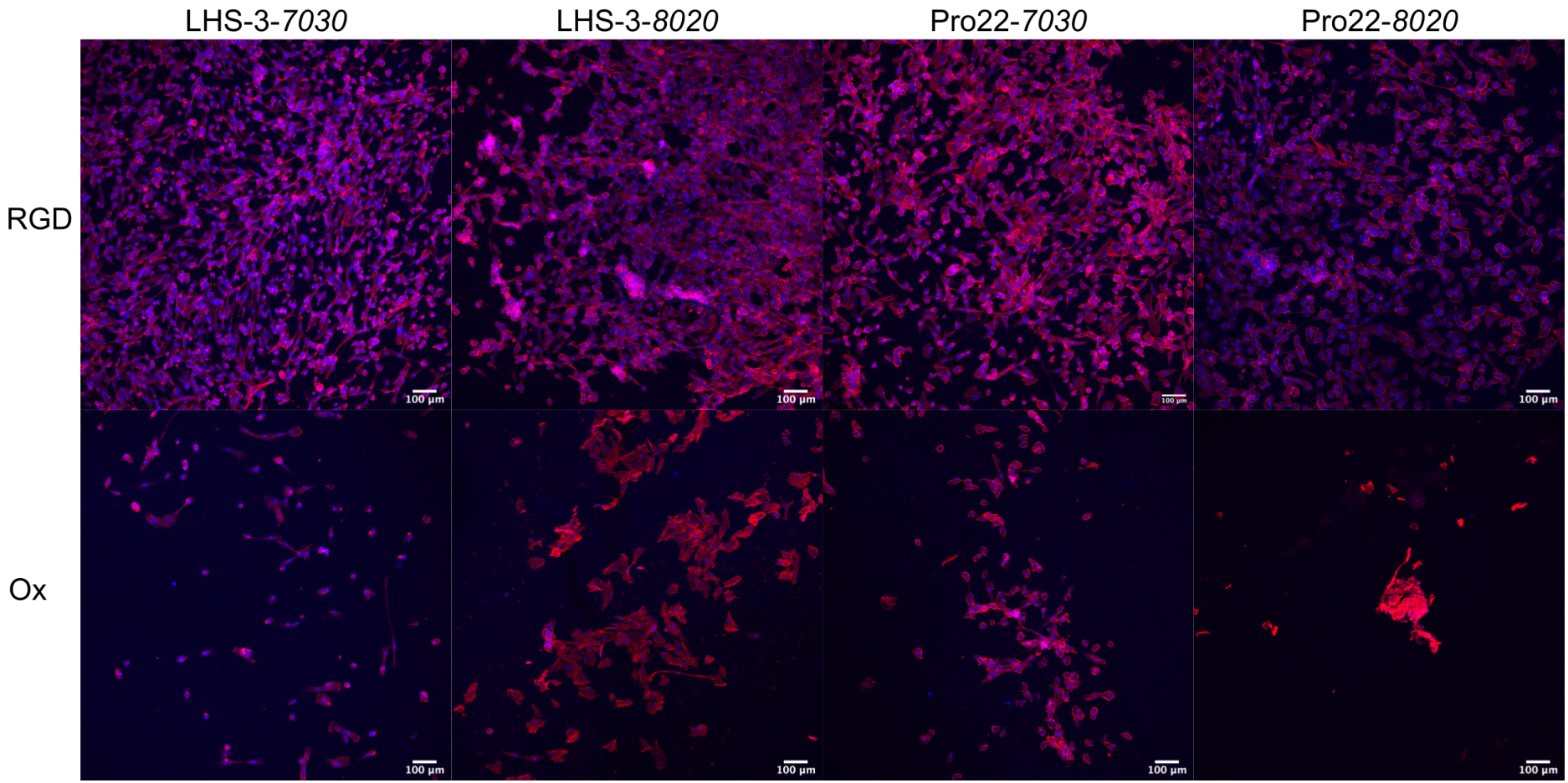

Figure 20 Processed CLSM images of NHDF cells seeded on eight crosslinked bioink disks. The labels on to the left indicate whether the bioink was formulated with RGD coupled alginate (2.25% w/v) (RGD) or the negative control oxidized alginate (2.25% w/v) (Ox). The labels on top indicate the type of alginate used (LHS-3 or Pro22 at 0.75% w/v) and their TTC+M/alginate ratio (70/30 or 80/20). Cells were preserved and stained with Phalloidin 568 and DAPI to excite the cytoskeleton (red) and nucleus (blue) after incubation for 48 hours in a humidified incubator with 5% CO_2 and 37°C. Scale bars correspond to 100 µm.

3.5 Morphological analysis of NHDF cells seeded on bioprinted bioinks

3.5.1 Short-term incubation

NHDFs were seeded on eight bioprinted grid scaffolds to investigate their adhesion behavior and morphology after a short-term incubation of 48 hours. The CLSM images of the initial investigation of the cell seeded scaffolds are presented in Appendix E. Because it was hard to differentiate whether the cells had adhered to the scaffold or the well bottom in all four images, the scaffolds were gently turned upside down and relocated to new wells.

Figure 21 shows the scaffolds and stained NHDF cells. While both the actin and nuclei were stained, only phalloidin appears to be excited. All eight scaffolds exhibit cell attachment, however, the negative controls with oxidized alginate had significantly fewer and more clustered cells. Cells seeded on RGD coupled bioinks had spread, covering large areas, and displayed elongated, spindle-shaped morphologies. The top portion of all four RGD composed scaffolds had areas without cells attached. This was particularly prominent for LHS-3-*8020*RGD and Pro22-*7030*RGD at the inner section of their grid lines. LHS-3-*7030*RGD and Pro22-*8020*RGD only had cells attached to the inner walls of the grids. Pro22-*8020*RGD scaffolds experienced some damage during the relocation to a new well. This can be seen in the image of the scaffold where the inner wall has been deformed in the bottom right corner.

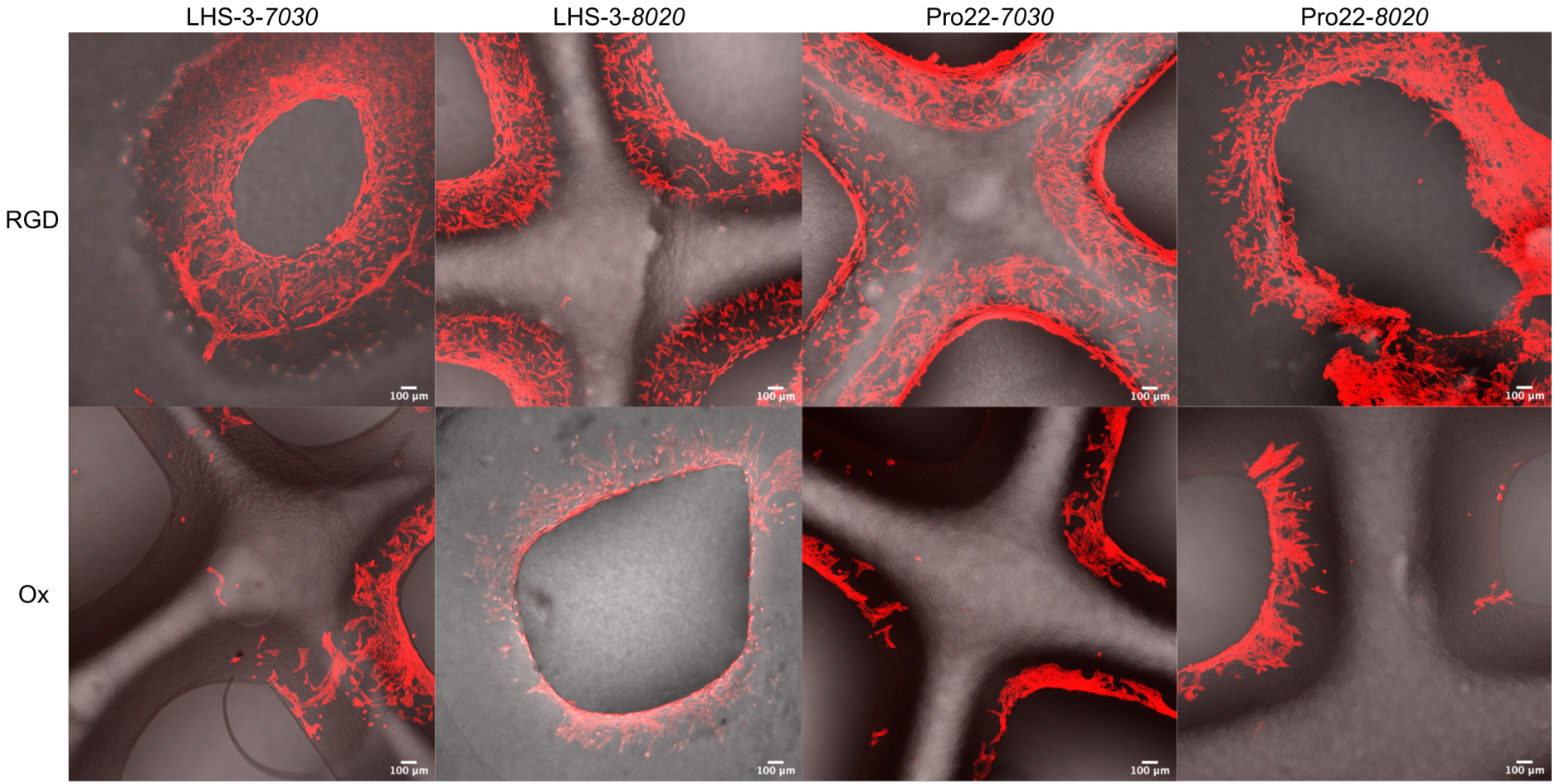

Figure 21 Processed CLSM images of NHDF cells seeded on eight bioprinted scaffolds. The labels to the left indicate whether the bioink was formulated with RGD coupled alginate (2.25% w/v) (RGD) or the negative control oxidized alginate (2.25% w/v) (Ox). The labels on top indicate the type of unmodified alginate used (LHS-3 or Pro22 at 0.75% w/v) and their TTC+M/alginate ratio (70/30 or 80/20). Cells were preserved and stained with Phalloidin 568 and DAPI to excite the cytoskeleton (red) and nucleus (blue) after incubation for 48 hours in a humidified incubator with 5% CO_2 and 37°C. Nuclei were not excited in these images. Scale bars correspond to 100 µm.

3.5.2 Long-term incubation

NHDF cells were cultured for 14-days on bioprinted scaffold grids produced using LHS-3-*7030*RGD. CLSM was used to investigate cell morphology after 14-day incubation to see how the cells adhered and spread across the scaffold after a longer incubation period. Figure 22 presents the CLSM images of four replicates (A-D) of the cell-laden scaffolds. Cells had adhered to and spread across the surface of all four scaffolds, however, there were also areas with fewer cells or no cells. The cells in Figure 22 A and C were elongated, and it was possible to distinguish between individual cells in some areas. In Figure 22 B and D, cells appeared to have populated the scaffold sufficiently, revealing denser cell networks. In some areas, cells also appear to grow on top of each other. This is better visualized in Appendix F.

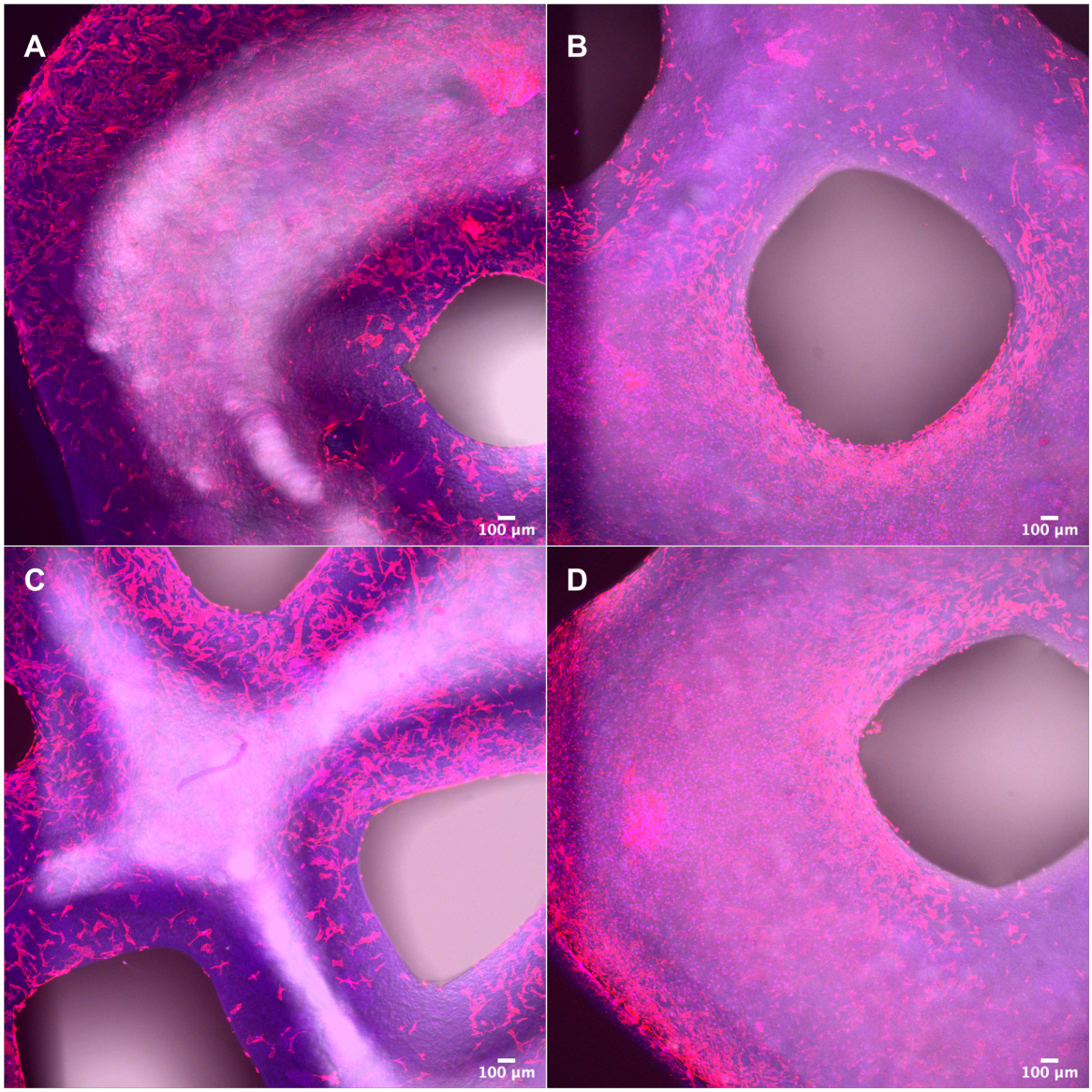

Figure 22 Processed CLSM images of NHDF cells seeded on bioprinted scaffolds composed of LHS-3-*7030*RGD. A, B, C and D refers to the different replicates imaged. Cells were preserved and stained with Phalloidin 488 and DAPI to excite the cytoskeleton (red) and nucleus (blue) after incubation for 14 days in a humidified incubator with 5% CO_2 and 37°C. Scale bars correspond to 100 µm.

3.6 Cell guidance by dual head 3D-bioprinting

A dual head bioprinting experiment was conducted to see if it was possible to guide the adhesion of NHDF cells by using two different bioinks. This involves the use of a hybrid construct being generated, involving the use of both RGD functionalized alginate and alginates free of any cell adhesion motifs. Figure 23 A shows the scaffold before and after gelation. Figure 23 B (left to right) shows the processed CLSM tile scans where the blue channel excited nuclei of the seeded NHDF cells, red channel excited cytoskeletons of the NHDF cells and merged channels of nucleus, cytoskeletons and brightfield of the spiral. Tile scans were performed to get an overview of the cell distribution across the entire bioprinted construct. Cells had adhered mostly to the RGD coupled bioink, however, cell adhesion was also seen to the oxidized bioink. Of note, significantly fewer cells were observed on the surface of the printed structures compared with previous experiments described in 3.5.1 and 3.5.2.

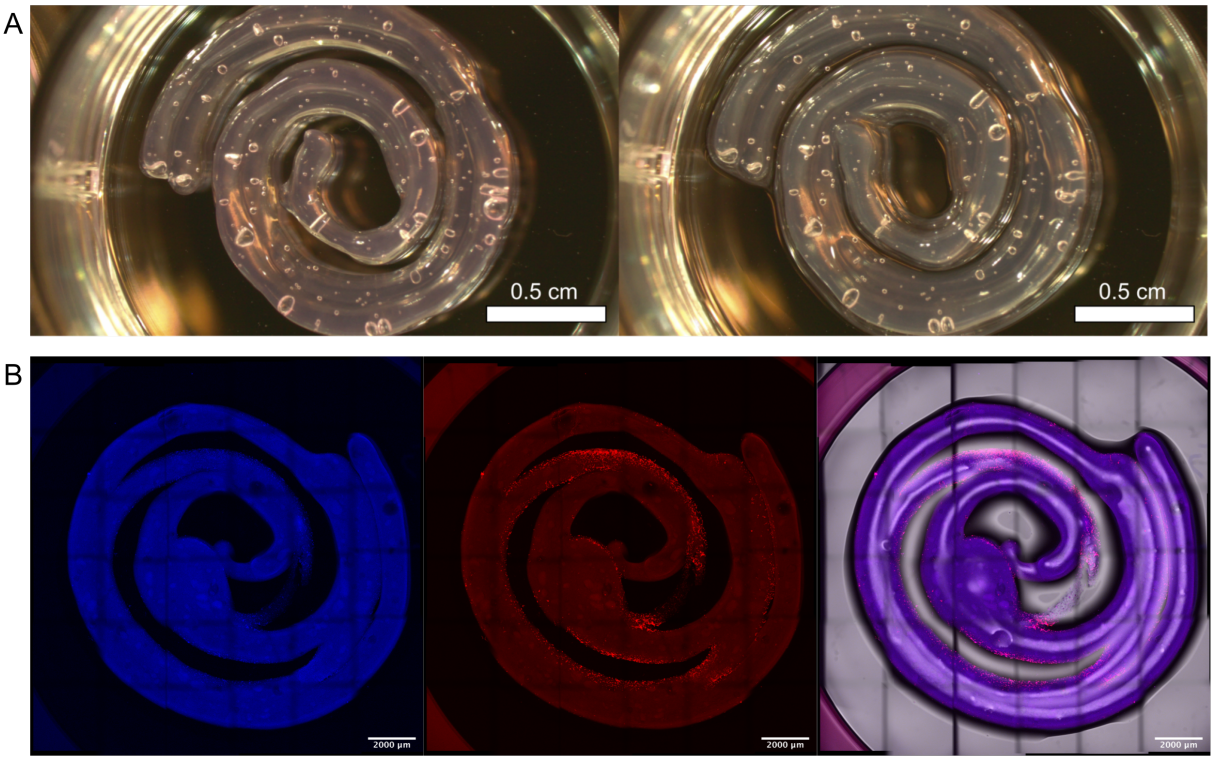

Figure 23 **A** Dual head bioprinted spirals before and after gelation, respectively. The inner spiral was bioprinted by PH3 loaded with LHS-3-*7030*RGD while the outer spiral was bioprinted by PH4 loaded with LHS-3-*7030*Ox. Scale bars correspond to 0.5 cm. **B** CLSM images of maximum composition merged tile scans of a replica of the same spiral as in A. This spiral was seeded with NHDF cells which were stained with Phalloidin (cytoskeleton staining with red fluorescent) and DAPI (nucleus staining with blue fluorescent) and preserved after three days of incubation in a humidified incubator with 5% CO_2 and 37°C. First picture from the left is the blue channel where the nuclei were excited. The image in the middle is the red channel where cytoskeletons were excited. Left image is a merge of the red, blue, and grey channels. Scale bars correspond to 0.2 cm.

4. Discussion

4.1 Preliminary studies

Before proceeding with further research, it was necessary to become acquainted with the 3D-bioprinter, biomaterials, and tools. As a result, a preliminary study was conducted, laying the groundwork for future decisions by optimizing techniques and methods. Some decisions and optimizations were made early on, while others had to be made during or between experiments.

The four different alginates studied in this thesis were selected to assess the impact of molecular weight and guluronic acid content. TTC and TTC+M were used in the experiments due to their high inherent purity, availability in medical-grade preparations, and relatively transparency compared with other nanocelluloses, which enabled easier visualization of cells. TTC was used in the biomaterial characterization studies while the medical grade TTC+M was used in cell experiments, as they were structurally equivalent and only differed in endotoxin content. NHDF cells were selected based on previous studies performed at NTNU and SINTEF where the cells demonstrated good viability and spreading in RGD-coupled alginate hydrogels (unpublished data). The varied TTC-alginate ratios were qualitatively observed during and after the printing process, revealing early on that the alginate's molecular weight and observed viscosity influenced the mixed bioinks. Low molecular weight alginates were thus ruled out early on. It was also observed that a high relative ratio of TTC to alginate (>60/40) was necessary to maintain the resolution of the printed structures. Various printing parameters were also investigated and optimized during these studies. Extrusion-based bioprinting was investigated using both a velocity-controlled syringe pump (PH3) and air pressure (PH4). Due to the need for fine-tuning of the air pressure when changing bioinks in PH4 was PH3 subsequently used. The continuous pressure in PH3 also made the bioprinting of scaffolds more reproducible, as this method demonstrates less dependence on bioink viscosity. The inkjet-based printer head CF-300H (PH1) (RegenHU, Switzerland) was investigated to see if cell seeding could be performed with it, but it was dismissed due to the relatively large volumes of cell suspension required. As a result, pipetting was used to seed the cells on top of bioprinted scaffolds.

Three different conical nozzles (250 µm, 410 µm and 580 µm) were investigated. Data simulations in Müller et al. (24) indicated that shear stress ranges above 160 Pa affected cell viability and that conical nozzles demonstrated lower shear stress on the cells than straight nozzles. The 410 µm conical nozzle was selected for further use as this was measured below

that range (24) and printed at high resolution in this study. The grid design of the scaffolds was used in the experiments to obtain a large surface area while only two vertical layers were printed to allow sufficient transparency for microscopy.

4.2 Biomaterial characterization

4.2.1 The importance of viscosity

As seen in Figure 11, the high molecular weight alginates LHS-3 (310 kDa) and Pro22 (360 kDa) demonstrated higher viscosities than the low molecular weight alginates LHS-9 (220 kDa) and 750PolyG (180 kDa), which was also apparent by visual inspection of the solutions. This was an expected result as the viscosity of dissolved alginates increase with molecular weight and concentration (6). The low molecular weight alginate 750PolyG showed a shear-thinning behaviour at all three concentrations as the viscosity decreased when the shear rate was increased. In polymer solutions, this can be caused by disentanglement of aggregates and/or alignment of the polymers with the direction of the deformation (39), but is generally not observed for alginates and was thus unexpected. Apart from the apparent shear-thinning, the viscosity was also lower than expected compared to LHS-9. This could indicate that there were impurities in the 750PolyG alginate samples, but additional rheological measurements and characterization of the alginates should be conducted to verify the results. Although shear-thinning is a desired property of bioinks (39), the low molecular weight alginates were not used further in this study because their low viscosities interfered with the mechanical properties of TTC when mixed in the preliminary studies. This was qualitatively observed as the bioinks showed poor printing resolution and the printed scaffolds began to “flow” before they were crosslinked.

When the highest alginate concentrations were compared in Figure 12, the LHS-3 and Pro22 at 3% (w/v) showed identical shear viscosities which can be explained by their similar molecular weights at 310 kDa and 360 kDa, respectively. Based on their high viscosities, high G-content, and their performance in the preliminary studies, the kelp alginate LHS-3, and the bacterial alginate Pro22 were selected for the subsequent formulation of bioinks. It was also of interest to see if the differences in G content resulted in an effect on the cell response.

As seen in Figure 13, all six bioinks composed of LHS-3 or Pro22 at 3% (w/v) mixed with TTC at three different ratios demonstrated good shear-thinning properties with similar flow curves

to the curves of TTC. The shear-thinning effect is a desired property of bioinks as the disentanglement of the polymers reduces the viscosity and therefore stress within the bioinks during flow (39). This is especially important for extrusion based bioprinting (EBB) where cells loaded in bioinks will be exposed to mechanical stress which can affect their viability (42). The bioinks should also have a rapid structural recovery to retain its shape after the printing process (43) and produce homogenous and consistent filaments which can be indicated by the consistent shear-thinning profiles.

The shear viscosity of the bioinks was influenced by the final alginate concentration as the flow curves decreased with increased alginate ratios. However, in both graphs in Figure 13, the 70/30 and 80/20 ratios with a final alginate concentration of 0.9% and 0.6%, respectively, demonstrated almost identical flow curves. The viscosity was affected to a greater extent by the 60/40 ratios with a final alginate concentration of 1.2%. There was also a difference between the LHS-3 and Pro22 bioinks, where the Pro22 had less impact on the rheological properties of TTC than the LHS-3. The difference in their molecular weights can explain this. In an earlier study conducted by Markstedt et al. (19) it was found that the viscosities of bioinks were more dependent on the dry content of bioinks (NFC and alginate concentrations) rather than the ratios of NFC and alginate. This is consistent with the findings in both the preliminary studies and the viscosity measurements, which show that the alginate selection (molecular weight and concentration) is more important than the final concentration of alginate in the bioink.

The viscosity was only measured in the bioinks composed of unmodified alginates, while the bioinks used in cell experiments were mixed with RGD coupled or oxidized alginates. There were not seen any critical differences in printability during these experiments, but it is natural that the modified alginates influenced the viscosity as their molecular weight and G-content varied from the unmodified alginates.

4.2.2 Mechanical properties of bioinks before and after gelation

The viscoelastic properties of LHS-3 and Pro22 bioinks with 60/40, 70/30 and 80/20 ratios investigated in Figure 14, demonstrated that all three ratios of both alginate-bioinks had a higher measured storage modulus (G') than loss modulus (G''). This indicated that they all were dominated by the elastic behaviour which is a desired property of bioinks as this indicates a stable, gel-like state (39). These results correlate with frequency sweep measurements in both Markstedt et al. (19) and Im et al. (41) which also investigated the viscoelastic properties of

alginate and NFC-based bioinks. However, the 60/40 and 70/30 ratios exhibited more similar properties than the 70/30 and 80/20 ratios. Because it is unknown why, an additional measurement should be carried out to validate the results and rule out the possibility of instrument variations. Regardless, all three bioink ratios demonstrated similar mechanical properties and the TTC exhibited stable structural properties that were not heavily affected by changes in final alginate concentration.

The gelation curves in Figure 15 showed that G' and G'' of all four bioinks (LHS-3-*7030*Ox, LHS-3-*8020*Ox, Pro22-*7030*Ox and Pro22-*8020*Ox) rapidly increased after the addition of 0.1M $CaCl_2$ and gradually turned into increasing asymptotic lines. G' and G'' did not show crossover and G' > G'' for all four bioinks, indicating strong elastic gels. During the 60-minute period, the phase angles (δ) gradually decreased, reaching a δ less than 5°. Smidsrød et al. (40) defined that measurements below 45° are largely elastic, demonstrating that the crosslinked bioinks were strong viscoelastic solids with a δ below 5°.

The 70/30 TTC/alginate ratios in both graphs in Figure 15 demonstrated greater mechanical strength than the 80/20 ratios. This was an expected result as the final alginate concentrations naturally impact the mechanical strength after crosslinking (19). Pro22 bioinks demonstrated a greater mechanical strength than LHS-3 bioinks, where the 80/20 ratio of Pro22 approached the mechanical strength of the 70/30 LHS-3. The greater G-content of Pro22 can explain this, as the crosslinked junctions by long continuous G-blocks function as reinforcement bars in the hydrogels, resulting in a higher mechanical rigidity when crosslinked (27). This can allow a lower alginate to TTC ratio, which in turn can improve the homogeneity of extruded filaments and resolution of printed structures.

The difference in mechanical rigidity was interesting to investigate further as previous research has demonstrated that when cells are encapsulated in bioinks, dense polymer networks may hinder cell migration, growth, and differentiation (6). Cells that are not encapsulated but seeded onto substrates, on the other hand, have in earlier studies showed durotaxis (44). Durotaxis is a phenomena where, when given the option, cells preferentially migrate to stiffer surfaces (45). Therefore, it was expected that the LHS-3 bioinks would be more suitable for cell encapsulation while the Pro22 bioinks would be better suited for cell seeding. Also, there was expected a difference in cell viability and cell adhesion between the two ratios since the 80/20 ratios demonstrated lower mechanical rigidity than the 70/30 ratios.

After the gelation measurements, it was discovered by observation that the inner portion of the samples had not been completely crosslinked. This may have affected the rheological measurements and could have been prevented by using an internal gelation method, allowing more homogeneous crosslinking through pH-driven release of uniformly distributed Ca^{2+} ions from $CaCO_3$ in gels (27). However, external gelation (diffusional setting) was used for the crosslinking of scaffolds and was therefore also used to measure their gelation. As the elastic modulus seemed to still increase after the 60-minute gelation is there a possibility that different results would have been seen if the bioinks were allowed to reach their gelation plateau. As a result, an additional study with longer gelation and measurement time should have been conducted to verify the results.

4.2.3 Stability test of bioprinted scaffolds

Two stability experiments of crosslinked scaffolds incubated in PSS at 37°C were carried out: one with unmodified alginates (60/40, 70/30, and 80/20 TTC/alginate) for 6 days, and another with oxidized alginates (70/30 and 80/20 TTC/alginate) for 7 days. During the incubation periods, none of the scaffolds showed visible structural alterations. The unmodified scaffolds appeared to be more transparent on day 6, although this was most likely due to the shift in light rather than Ca^{2+} ion diffusion.

The high stability of the 3D-bioprinted grid scaffolds is facilitated by the high G-content of the alginates (27). Ochbaum et al. (46) performed rheological measurements on alginate hydrogels immersed in phosphate buffered saline (PBS). Ions from the PBS were expected to gradually wash out Ca^{2+} ions from the crosslinked hydrogels and naturally affect the physical properties of their gels. The measurements confirmed that all tested gels were weakened (46). Even though there was no visual swelling or dissolution of the scaffolds in this thesis (incubated in PSS), a rheological measurement could have revealed a reduction in mechanical strength based on replacement of calcium in crosslinking junction zones with sodium ions. To accelerate the dissolvement of the scaffolds could sodium citrate be added to the medium in a controlled manner. Citrate ions would then chelate to the calcium ions crosslinked between the alginate polymers, causing the alginate to dissolve (47).

The apparent phase separation of the LHS-3-*6040* and Pro22-*6040* can be explained by the gelation method used where the Ca^{2+} ions are diffused into the scaffold. This can result in an uneven distribution of alginate and TTC where a sharp gelling zone is created at the surface

and alginate molecules diffuse from the centre part of the scaffold (27). The 60/40 ratio was excluded from further investigations due to their poorer printing resolution, and their lack of homogeneity.

4.3 Cell-biomaterial interaction studies

LHS-3-*7030*, LHS-3-*8020*, Pro22-*7030* and Pro22-*8020* with RGD-coupled or oxidized alginate were used for studying cell-biomaterial interactions. These bioinks were chosen due to their superior printability, homogeneity, and gelation, demonstrated in the biomaterial characterization studies.

Cells cultured *in vitro* are known to respond to the physical and chemical cues provided by their microenvironments. In the context of experiments presented in this thesis, apart from the chemical compositions among the hydrogels, physical parameters such as dimensionality (2D and 3D), geometry (shape), topography and stiffness are important to consider. For this reason, cell-biomaterial interaction studies in this thesis address how the formulated bioinks influenced NHDF cells when they were both encapsulated within the bioinks (3D) prior to crosslinking, as well as when they were seeded onto bioink scaffold surfaces (2D/2.5D).

4.3.1 NHDF cells loaded in bioinks

In both the 7-day and 14-day cultures, NHDF cells showed good overall viability. Cell viability data for the different bioinks are presented as percentages relative to the total amount of cells present within the gel disk. The results demonstrated that none of the bioink formulations were toxic to the cells, with higher than 70% viability in all formulations. While it would also be useful to compare final cell numbers between the different bioink formulations and incubation periods for signs of proliferation, due to the large initial variability in cell numbers during production, this data set would unfortunately not provide an accurate comparison of bioinks due to an initial variability in cell numbers during casting of the disks.

Dense polymer networks with high mechanical rigidity have been shown to limit cell migration and growth (6). As seen in Figure 15 the bioinks in this study demonstrated different mechanical rigidity when crosslinked, thus a difference in cell viability between the bioinks was thought to be observed. However, there was no observable relationship between cell viability, cell morphology and the mechanical properties of the bioinks. As a result, the formulated bioinks

in this study were within a range of rigidity which allowed for good printability as well as cell biocompatibility. Similar properties are reported as a traditional biofabrication window, where hydrogel properties are adjusted to fit both the shape fidelity in biofabrication as well as biocompatibility with cells (37). Additionally, there were no significant differences between viability in RGD coupled bioinks compared to the negative controls with oxidized alginate. The same results have been observed when olfactory ensheathing cells (OECs) and myoblasts were cultured in microbeads composed of RGD-coupled alginate gels, which showed no enhanced survival attributing to the RGD grafting (48). This suggests that the RGD-coupling of alginate alone is not sufficient for the cells to thrive when encapsulated. Nonetheless, this observation is particularly interesting since fibroblasts are known to be an adhesion-dependent cell type of mesenchymal linage (14). One explanation for RGD-coupling not being a prominent factor for NHDF cell survival could be related to the physical restriction the hydrogel imposes onto the cells when embedded in these gels (6). The lack of cell-degradability in these scaffolds likely restricts cells to migrate and replicate, while potentially leaving cells in a senescent-like state. To reduce the physical restriction, matrix metalloproteinase (MMP)-sensitive peptides could be incorporated into the bioinks. MMP-sensitive peptides facilitate a cell-driven mechanism for alginate hydrogel degradation (49), and could potentially increase the viability and migration of the encapsulated NHDF cells.

During the crosslinking of the bioink disks, cell loaded Pro22-*8020*Ox dissolved into the $CaCl_2$ solution during crosslinking. This likely occurred due to the addition of too high concentration of cell suspension compared to bioink, which can cause physical blocking of crosslinking binding sites (39). It was not attempted to formulate a new Pro22-*8020*Ox as redoing the material formulation and using cells with a different passage number and concentration could have complicated direct comparison with the other bioinks.

Advancement of the bioink towards a cellular microenvironment may potentially include cell adhesive proteins that are commonly found in the ECM, such as collagen, laminin, or fibronectin. There is no doubt that attempting to replicate the extremely complex ECM network is an ambitious task to support cell colonisation. However, a more viable approach was to investigate how the bioinks could function as a template for cell adhesion. It was therefore subsequently studied how the NHDF cells adhered and spread when seeded on the surfaces of bioink scaffolds.

4.3.2 NHDF cells seeded on casted and 3D-bioprinted scaffolds

Before the RGD-coupled bioinks were 3D-bioprinted, casted bioink disks were seeded with NHDF cells and investigated to determine if the RGD was functional when mixed with the unmodified alginates and TTC+M. Cell adhesion and spreading on the RGD-coupled disks were successful, as shown in Figure 20, with a significant difference from the negative controls made with oxidized alginate. The clustering of cells on the negative controls indicated that the cell-cell interactions were stronger than the cell-biomaterial interactions and demonstrated that the oxidized bioinks did not support cell adhesion. This has also been seen in an earlier study where NHDF cells aggregated and formed clusters on pure alginate hydrogels (50). As cells cannot adhere to alginate without cell adhesion molecules (51) this was an expected result, but also showed that a relatively small amount of RGD-coupled alginate in a homogenous mixture with unmodified alginate and cellulose was sufficient to induce adhesion of NHDF.

There is an interrelated relationship between substrate stiffness, RGD-content, and the adhesion of cells. If the scaffold is not sufficiently stiff, the presence of RGD alone will not promote cell spreading (52). The RGD concentration of the bioinks in this study were estimated in Appendix G to 1.5 mM in the 80/20 ratios and 1.7 mM in the 70/30 ratios. As the seeded cells in Figure 20 showed spreading, the scaffold disks were sufficiently stiff and the RGD concentration was high enough for the cells to adhere on all four casted disks. In other studies, the stiffness of the material surface has been an important factor for cell adhesion (53). As the rheological measurements of crosslinked bioinks indicated that Pro22 bioinks were stiffer than LHS-3 bioinks, and the 70/30 ratios were stiffer than the 80/20 ratios, it was expected to see a difference in cell adhesion to the different bioinks. However, as seen in the cell viability experiment, the difference in mechanical rigidity did not appear to be critical for the cells; similarly, no significant differences of cell adhesion to the different RGD-coupled bioinks were observed in the cell seeding experiments. As the difference in cell adhesion was not significant between the different cellulose-to-alginate ratios, all bioinks were therefore included in the short-term (48 H) 3D-bioprinting experiment where initial cell adhesion to grid scaffolds was investigated.

When cells were seeded on the casted disks, a drop of cell suspension was pipetted onto the disk surfaces. The surface tension kept the drop from collapsing to the bottom of the well, allowing cells to adhere for an hour before medium was added. This method was also used to seed cells onto 3D-bioprinted grid scaffolds, but because the grid scaffolds did not have flat 2D

surfaces, most of the cell suspension fell to the well's bottom. As seen in Figure 21, cells had successfully adhered to the grid scaffolds despite this challenge. This was seen by the stained cytoskeletons, but the DAPI used to stain the cell nucleus was not visible in Figure 21. This is most likely due to the fixed cell-laden scaffolds being stored for a period before imaging with CLSM. Despite cells adhering to the grid scaffolds successfully, certain measures could increase the overall cell attachment. For instance, the incorporation of a multi axes rotary device that distributes the cells across the scaffold during incubation may lead to better cell adhesion (54).

Interestingly, as shown in Figure 21, the cells had mostly adhered to the inner walls or junctions of the grids in the short-term (48H) experiment. As physical features of the microenvironment affect cells, and mechanical and topological characteristics can cause morphological alterations (55), the initial cell adhesion to the inner junctions may be linked to the geometry of the grid scaffolds. In a study conducted by Park et al., mouse fibroblasts were studied in convex and concave microenvironments. This study demonstrated that the cells actively escaped concave structures while climbing onto the convex structures was not a problem (55). This can be relevant for the results in Figure 21 as the curvature on top of the scaffolds might have been too concave for the cells during the initial adhesion, causing them to adhere to the inner junctions. This was also seen in the negative controls with bioinks composed of oxidized alginate where most of the imaged cells formed clusters by the junctions. This indicated that the junction zones had better physical properties for the adhesion of NHDF cells than the top of the grid scaffolds.

Because all RGD-coupled bioinks demonstrated similar cell adhesion and proliferation, it was suggested that either bioink could be used for long-term cultivation. The choice of LHS-3-*7030*RGD was made since LHS-3 was readily available, and the higher RGD concentration in 70/30 compared to 80/20 was expected to provide the cells with a good foundation for adhesion to the scaffolds. As seen in Figure 22, the cells had adhered and spread across the LHS-3-*7030*RGD grid scaffolds during the long-term (14-day) incubation. They had not only adhered to the top of the scaffolds, which had not been seen in the initial adhesion experiment, but they also appeared to have grown on top of each other in some areas at two of the replicates. This suggests that the cells managed to spread to the more concave areas of the scaffolds during the longer incubation period.

4.4 Cell guidance by dual head 3D-bioprinting

The dual head 3D-bioprinted spirals in Figure 23 A were successfully bioprinted as designed in BioCAD™. However, as seen in Figure 23 B, even though the number of seeded cells was almost doubled, significantly fewer cells were observed compared to the 3D-bioprinted grid scaffolds. Several optimizations of the experiment should be investigated in an additional study. Some of these are presented as follows. The cells used in this study had shown signs of poor adhesion and growth during the cultivation in culture flasks. They were also at passage 15 which is the last passage number before the cells are no longer used in experiments. This may have affected the adhesion to the spiral scaffolds in this experiment, resulting in few adhered cells. As the cells in 3.5.1 had mostly adhered to junctions of the bioprinted grid scaffolds, the initial adhesion may have been affected by the rounded concave geometry of the bioprinted spirals, resulting in several cells being washed away when media was added. The BioCAD design can therefore be improved by creating a tighter scaffold where the inks connect with each other, resulting in more grooves and convex areas that the cells can adhere to. As this experiment was a proof of concept for cell guiding, this indicates that the idea of guiding cells by dual head 3D-bioprinting is feasible, but that optimization of the experimental design is needed.

4.5 Future perspectives

In addition to optimization of the spiral design, other types of hybrid scaffolds could be explored to study material-cell interactions and cell guiding. It would be interesting to investigate this further because the shape of the scaffolds appeared to have a large influence on cell adhesion. The geometries of the scaffolds designed in Figure 24 can be used for this purpose. The BioCAD-design on the left will most likely produce rounded bioink filaments with poor cell adhesion, whereas the design on the right will most likely produce a 2.5D surface with small concave grooves, promoting cell adhesion. As a result, these designs are proposed for further research into cell adhesion on scaffold geometries.

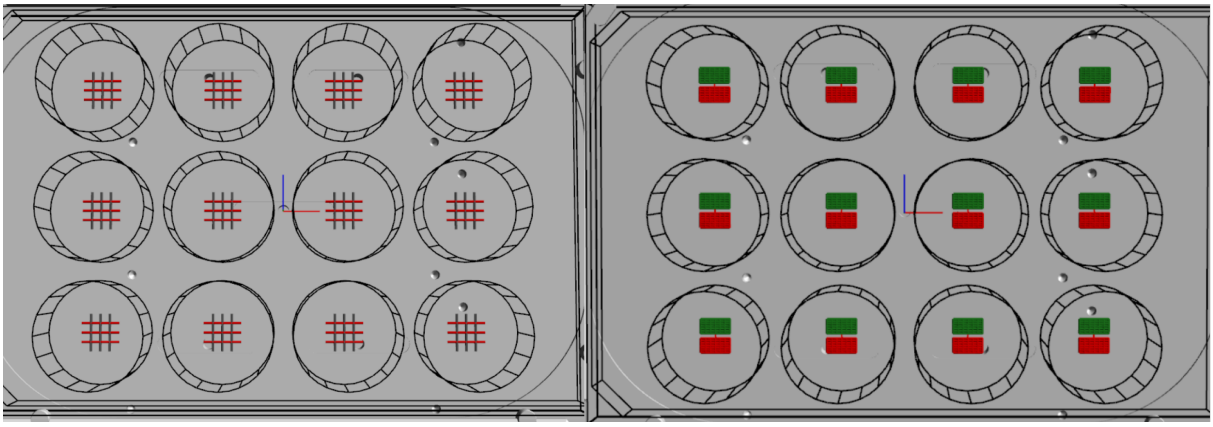

Figure 24 Dual head bioprinting designs proposed for further studies. The scaffolds are designed to be printed with two different printheads indicated by the different colors of the different deposited materials (red and green). Designed in BioCAD™ and visualized in 3D Print Preview.

Pontiggia et al. (56) recently demonstrated a proof of concept that by 3D-bioprinting various skin derived cells mixed in collagen hydrogels, a large-scale human skin substitute could be functional *in vivo*. Therefore, another possible application of the bioinks is to encapsulate different cell types i.e., cells derived from the different layers of the skin, and 3D-bioprint a layered scaffold to resemble human skin tissue. With longer incubation period, the cells in the different layers might eventually interact with each other and form *in vitro* tissue-like constructs. However, this will probably require optimizations of the bioinks, such as the addition of growth-enhancing proteins. The incorporation of MMP-sensitive peptides in the bioinks or the addition of citrate to the media can also be examined further to stimulate cell migration and accelerate scaffold dissolution (47, 49). Additionally, the cultivation method can be optimized by the implementation of a bioreactor or perfusion system to increase nutrient transfer (54). Especially for cells adhered onto the scaffold templates, a bioreactor can be used to facilitate the growth of neo tissue around the scaffolds (6).

5. Concluding remarks

In the present study, rheological properties of novel bioinks composed of functionalized alginates and nano fibrillated cellulose derived from tunicates (TTC) were successfully characterized for use in 3D-bioprinting and demonstrated biocompatibility with NHDF cells. Four different alginates were investigated by rheological measurements and quantitative observations. The mechanical properties of the formulated bioinks were highly dependent on the choice of alginate, and the two alginates LHS-3 and Pro22 at 3% (w/v) with high molecular weight and guluronic acid content, demonstrated the best suited viscosities for subsequent mixing with TTC to formulate bioinks.

The formulated bioinks demonstrated rheological properties suitable for 3D-bioprinting. The TTC provided a stable carrier system where the viscoelastic behaviour of the bioinks prior to crosslinking was not greatly affected by final concentrations and types of alginates. However, the 60/40 bioinks demonstrated an uneven distribution of alginate and TTC after crosslinking, prompting further investigation of the 70/30 and 80/20 ratios. Gelation measurements and stability tests of both Pro22 and LHS-3 bioinks demonstrated that they had similar viscoelastic properties and high mechanical strength. The high G-content in the Pro22 bioinks narrowed the difference in mechanical rigidity between the 70/30 and 80/20 ratios. The use of high-G alginates can thus be favourable because it allows greater flexibility in formulation without having a large impact on the final mechanical properties.

After 7 and 14 days of incubation, the encapsulated cells demonstrated cell viability above 70% in all bioink formulations. A significant difference in cell adhesion was observed between the bioinks formulated with RGD-coupled and oxidized alginates. No clear difference in cell adhesion was seen between the two alginate types and the two TTC-alginate ratios. A good cell response could thereby be achieved independently of alginate choice and mixing ratio. It was not concluded that cells could be guided by dual head bioprinting. However, there were indications of it, and it is recommended that the method be optimized to facilitate cell guiding.

References

1. Nikolic M, Sustersic T, Filipovic N. In vitro Models and On-Chip Systems: Biomaterial Interaction Studies With Tissues Generated Using Lung Epithelial and Liver Metabolic Cell Lines. Frontiers in Bioengineering and Biotechnology. 2018;6.
2. Haycock JW. 3D Cell Culture: A Review of Current Approaches and Techniques. In: Haycock JW, editor. 3D Cell Culture: Methods and Protocols. Totowa, NJ: Humana Press; 2011. p. 1-15.
3. Langhans SA. Three-Dimensional in Vitro Cell Culture Models in Drug Discovery and Drug Repositioning. Frontiers in Pharmacology. 2018;9.
4. de Dios-Figueroa GT, Aguilera-Marquez JdR, Camacho-Villegas TA, Lugo-Fabres PH. 3D Cell Culture Models in COVID-19 Times: A Review of 3D Technologies to Understand and Accelerate Therapeutic Drug Discovery. Biomedicines. 2021;9(6):602.
5. Elliott NT, Yuan F. A review of three-dimensional in vitro tissue models for drug discovery and transport studies. J Pharm Sci. 2011;100(1):59-74.
6. Malda J, Visser J, Melchels FP, Jüngst T, Hennink WE, Dhert WJA, et al. 25th Anniversary Article: Engineering Hydrogels for Biofabrication. Advanced Materials. 2013;25(36):5011-28.
7. Jensen C, Teng Y. Is It Time to Start Transitioning From 2D to 3D Cell Culture? Frontiers in Molecular Biosciences. 2020;7.
8. Mertgen A-S, Trossmann VT, Guex AG, Maniura-Weber K, Scheibel T, Rottmar M. Multifunctional Biomaterials: Combining Material Modification Strategies for Engineering of Cell-Contacting Surfaces. ACS Applied Materials & Interfaces. 2020;12(19):21342-67.
9. Alberts B, Johnson A, Lewis J, Raff M, Roberts K, Walter P. Molecular Biology of The cell. 6th ed. New York Garland Science 2015.
10. Ozbolat IT, Hospodiuk M. Current advances and future perspectives in extrusion-based bioprinting. Biomaterials. 2016;76:321-43.
11. In Situ Gelation for Cell Immobilization and Culture in Alginate Foam Scaffolds. Tissue Engineering Part A. 2014;20(3-4):600-10.
12. Ullah F, Othman MBH, Javed F, Ahmad Z, Akil HM. Classification, processing and application of hydrogels: A review. Materials Science and Engineering: C. 2015;57:414-33.
13. Chahal AS. From inert to active: biofunctionalised PEG hydrogels to guide stem cell behaviour. DUO vitenarkiv University of Oslo 2020.

14. Fernandes IR, Russo FB, Pignatari GC, Evangelinellis MM, Tavolari S, Muotri AR, et al. Fibroblast sources: Where can we get them? Cytotechnology. 2016;68(2):223-8.
15. Seluanov A, Vaidya A, Gorbunova V. Establishing primary adult fibroblast cultures from rodents. J Vis Exp. 2010(44):2033.
16. Green JA, Yamada KM. Three-dimensional microenvironments modulate fibroblast signaling responses. Adv Drug Deliv Rev. 2007;59(13):1293-8.
17. Aslantürk Ö. In Vitro Cytotoxicity and Cell Viability Assays: Principles, Advantages, and Disadvantages. 2018.
18. Jonkman J, Brown CM, Wright GD, Anderson KI, North AJ. Tutorial: guidance for quantitative confocal microscopy. Nature Protocols. 2020;15(5):1585-611.
19. Markstedt K, Mantas A, Tournier I, Martínez Ávila H, Hägg D, Gatenholm P. 3D Bioprinting Human Chondrocytes with Nanocellulose-Alginate Bioink for Cartilage Tissue Engineering Applications. Biomacromolecules. 2015;16(5):1489-96.
20. Rastogi P, Kandasubramanian B. Review of alginate-based hydrogel bioprinting for application in tissue engineering. Biofabrication. 2019;11(4):042001.
21. Axpe E, Oyen ML. Applications of Alginate-Based Bioinks in 3D Bioprinting. Int J Mol Sci. 2016;17(12).
22. Chen DXB. Extrusion Bioprinting of Scaffolds: An Introduction. In: Chen DXB, editor. Extrusion Bioprinting of Scaffolds for Tissue Engineering Applications. Cham: Springer International Publishing; 2019. p. 1-13.
23. Fang Y, Guo Y, Liu T, Xu R, Mao S, Mo X, et al. Advances in 3D Bioprinting. Chinese Journal of Mechanical Engineering: Additive Manufacturing Frontiers. 2022;1(1):100011.
24. Müller M, Öztürk E, Arlov Ø, Gatenholm P, Zenobi-Wong M. Alginate Sulfate-Nanocellulose Bioinks for Cartilage Bioprinting Applications. Ann Biomed Eng. 2017;45(1):210-23.
25. Christensen BE. Biopolymers. Trondheim: NTNU; 2014.
26. Draget KI, Moe ST, Skjåk-Braek G, Inulin OS, Franck A. Food Polysaccharides and Their Applications: Chapter 9 2ed. Stephen AM, Phillips GO, Williams PA, editors. Boca Raton: CRC Press; 2006.
27. Draget KI, Skjåk-Braek G, Smidsrød O. Alginate based new materials. Int J Biol Macromol. 1997;21(1-2):47-55.

28. Donati I, Paoletti S. Material Properties of Alginates. In: Rehm BHA, editor. Alginates: Biology and Applications. Berlin, Heidelberg: Springer Berlin Heidelberg; 2009. p. 1-53.
29. Gacesa P. Alginates. Carbohydrate Polymers. 1988;8(3):161-82.
30. Paques JP. Chapter 3 - Alginate Nanospheres Prepared by Internal or External Gelation with Nanoparticles. In: Sagis LMC, editor. Microencapsulation and Microspheres for Food Applications. San Diego: Academic Press; 2015. p. 39-55.
31. Hu T, Lo ACY. Collagen-Alginate Composite Hydrogel: Application in Tissue Engineering and Biomedical Sciences. Polymers (Basel). 2021;13(11):1852.
32. Kumar AS, Fletcher NL, Houston ZH, Thurecht KJ, Grøndahl L. Evaluation of the in vivo fate of ultrapure alginate in a BALB/c mouse model. Carbohydrate Polymers. 2021;262:117947.
33. Arlov Ø, Skjåk-Bræk G. Sulfated Alginates as Heparin Analogues: A Review of Chemical and Functional Properties. Molecules. 2017;22(5):778.
34. Coffey DI, Bell DA, Henderson A. Food Polysaccharides and Their Applications: Chapter 5 Cellulose. 2 ed. Stephen AM, Phillips GO, Williams PA, editors. Boca Raton: CRC Press; 2006.
35. Kjesbu JS, Zaytseva-Zotova D, Sämfors S, Gatenholm P, Troedsson C, Thompson EM, et al. Alginate and tunicate nanocellulose composite microbeads – Preparation, characterization and cell encapsulation. Carbohydrate Polymers. 2022;286:119284.
36. Kaffashsaie E, Yousefi H, Nishino T, Matsumoto T, Mashkour M, Madhoushi M, et al. Direct conversion of raw wood to TEMPO-oxidized cellulose nanofibers. Carbohydrate Polymers. 2021;262:117938.
37. Ouyang L. Pushing the rheological and mechanical boundaries of extrusion-based 3D bioprinting. Trends in Biotechnology.
38. Worldwide MI. Malvern Instruments White Paper-A Basic Introduction to Rheology Shear Flow. 2016.
39. Amorim PA, d'Ávila MA, Anand R, Moldenaers P, Van Puyvelde P, Bloemen V. Insights on shear rheology of inks for extrusion-based 3D bioprinting. Bioprinting. 2021;22:129.
40. Smidsrød O. Biopolymer chemistry. Moe ST, editor. Trondheim: Tapir Academic Press; 2008.
41. Im S, Choe G, Seok JM, Yeo SJ, Lee JH, Kim WD, et al. An osteogenic bioink composed of alginate, cellulose nanofibrils, and polydopamine nanoparticles for 3D

bioprinting and bone tissue engineering. International Journal of Biological Macromolecules. 2022;205:520-9.
42. Habib MA, Khoda B. Rheological analysis of bio-ink for 3D bio-printing processes. Journal of Manufacturing Processes. 2022;76:708-18.
43. Heggset EB, Strand BL, Sundby KW, Simon S, Chinga-Carrasco G, Syverud K. Viscoelastic properties of nanocellulose based inks for 3D printing and mechanical properties of CNF/alginate biocomposite gels. Cellulose. 2019;26(1):581-95.
44. Hopp I, Michelmore A, Smith LE, Robinson DE, Bachhuka A, Mierczynska A, et al. The influence of substrate stiffness gradients on primary human dermal fibroblasts. Biomaterials. 2013;34(21):5070-7.
45. Breuls RGM, Jiya TU, Smit TH. Scaffold stiffness influences cell behavior: opportunities for skeletal tissue engineering. Open Orthop J. 2008;2:103-9.
46. Ochbaum G, Davidovich-Pinhas M, Bitton R. Tuning the mechanical properties of alginate–peptide hydrogels. Soft Matter. 2018;14(21):4364-73.
47. Wu Z, Su X, Xu Y, Kong B, Sun W, Mi S. Bioprinting three-dimensional cell-laden tissue constructs with controllable degradation. Scientific Reports. 2016;6(1):24474.
48. Sandvig I, Karstensen K, Rokstad AM, Aachmann FL, Formo K, Sandvig A, et al. RGD-peptide modified alginate by a chemoenzymatic strategy for tissue engineering applications. Journal of Biomedical Materials Research Part A. 2015;103(3):896-906.
49. Fonseca KB, Gomes DB, Lee K, Santos SG, Sousa A, Silva EA, et al. Injectable MMP-Sensitive Alginate Hydrogels as hMSC Delivery Systems. Biomacromolecules. 2014;15(1):380-90.
50. Sarker B, Singh R, Silva R, Roether JA, Kaschta J, Detsch R, et al. Evaluation of fibroblasts adhesion and proliferation on alginate-gelatin crosslinked hydrogel. PLOS One. 2014;9(9):e107952.
51. Slaughter BV, Khurshid SS, Fisher OZ, Khademhosseini A, Peppas NA. Hydrogels in Regenerative Medicine. Advanced Materials. 2009;21(32-33):3307-29.
52. Chahal AS, Schweikle M, Heyward CA, Tiainen H. Attachment and spatial organisation of human mesenchymal stem cells on poly(ethylene glycol) hydrogels. Journal of the Mechanical Behavior of Biomedical Materials. 2018;84:46-53.
53. Espina JA, Marchant CL, Barriga EH. Durotaxis: the mechanical control of directed cell migration. The FEBS Journal. 2021.
54. Varley MC, Markaki AE, Brooks RA. Effect of Rotation on Scaffold Motion and Cell Growth in Rotating Bioreactors. Tissue Eng Part A. 2017;23(11-12):522-34.

55. Park JY, Lee DH, Lee EJ, Lee SH. Study of cellular behaviors on concave and convex microstructures fabricated from elastic PDMS membranes. Lab Chip. 2009;9(14):2043-9.
56. Pontiggia L, Van Hengel IAJ, Klar A, Rütsche D, Nanni M, Scheidegger A, et al. Bioprinting and plastic compression of large pigmented and vascularized human dermo-epidermal skin substitutes by means of a new robotic platform. Journal of Tissue Engineering. 2022;13:20417314221088513.

Appendix

A. Viscosity of low molecular weight alginate LHS-7

The flow curves of the three LHS-7 concentrations are shown in Figure 25. Despite being dissolved at high concentrations (6, 8, and 10% (w/v), LHS-7 (Mw = 44 kDa) had a low viscosity when compared to the other samples. The mechanical properties of bioinks composed of LHS-7 were negatively affected by the low viscosity and were therefore not printable. Because of these factors, LHS-7 was early ruled out as a candidate for subsequent 3D-bioprinting.

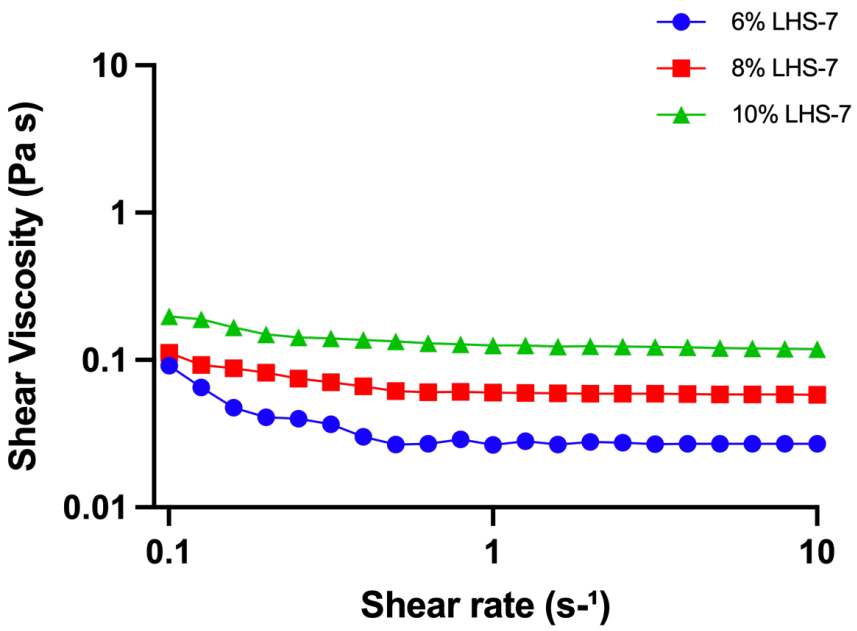

Figure 25 Flow curves of LHS-7 (44 kDa) at three concentrations. Shear viscosity (Pa s) was measured with shear rates from 0.1 s^{-1} to 10 s^{-1}.

B. Determination of LVR of six bioinks

Strain sweeps were performed to find the linear viscoelastic region (LVR) of the bioinks and to see how much strain and stress could be applied to the samples before their mechanical properties changed. The measurement also gave the optimal strain and stress for the samples which were further used in the frequency sweep tests.

Figure 26 shows the strain sweeps of the six bioinks. All bioinks showed a higher elastic modulus (G') than the loss modulus (G''), indicating solid- or gel-like behaviour. The end of the LVR of the bioinks was determined by the point at which the bioinks were affected by the

shear strain, i.e. when G' began to decrease. The G' of LHS-3 bioinks with TTC ratios of 60/40, 70/30 and 80/20 began to decrease at shear strains of 0.25%, 0.25% and 0.40%, respectively. The G' of Pro22 bioinks with TTC ratios of 60/40, 70/30 and 80/20 began to decrease at 0.20%, 0.25% and 0.25%, respectively. Due to poor signal-to-noise ratio, the first ten G' and G'' measurements for LHS-3-*6040* and LHS-3-*7030* were removed from the graph in Figure 26 A.

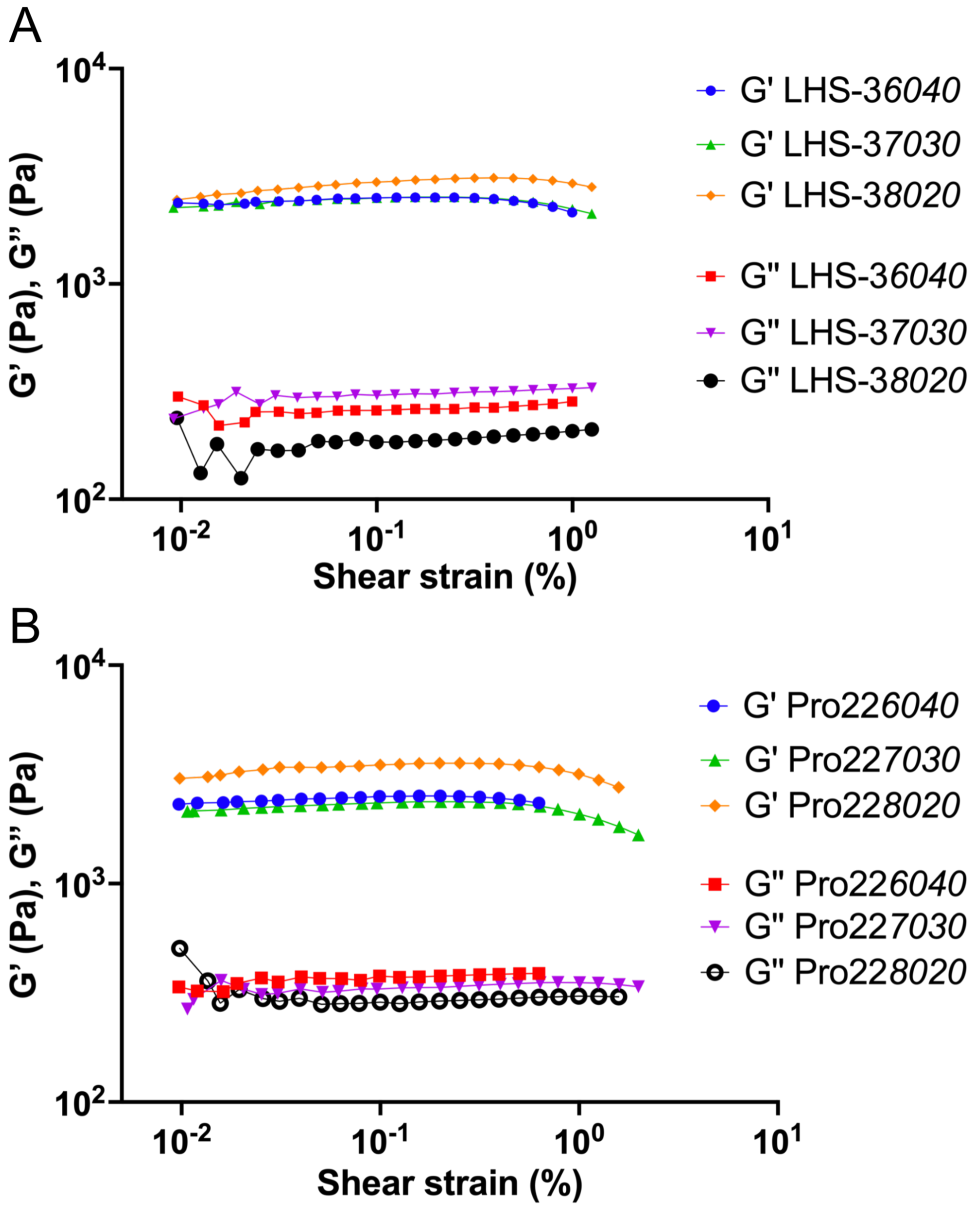

Figure 26 Amplitude strain sweeps of bioinks formulated of LHS-3 or Pro22 mixed with TTC at three different ratios (60/40, 70/30 or 80/20). Storage modulus (G') and loss modulus (G'') was measured with a shear strain (%) range from 0.1 % to 10^3 %. Frequency = 1 Hz. **A**: Strain sweeps of bioinks composed of LHS-3. **B**: Strain sweeps of bioinks composed of Pro22.

C. Image optimisation for cell counting

Dead cells inside or around bubbles were discovered during cell counting of encapsulated cells. These were excluded from cell counting using the method shown in Figure 27.

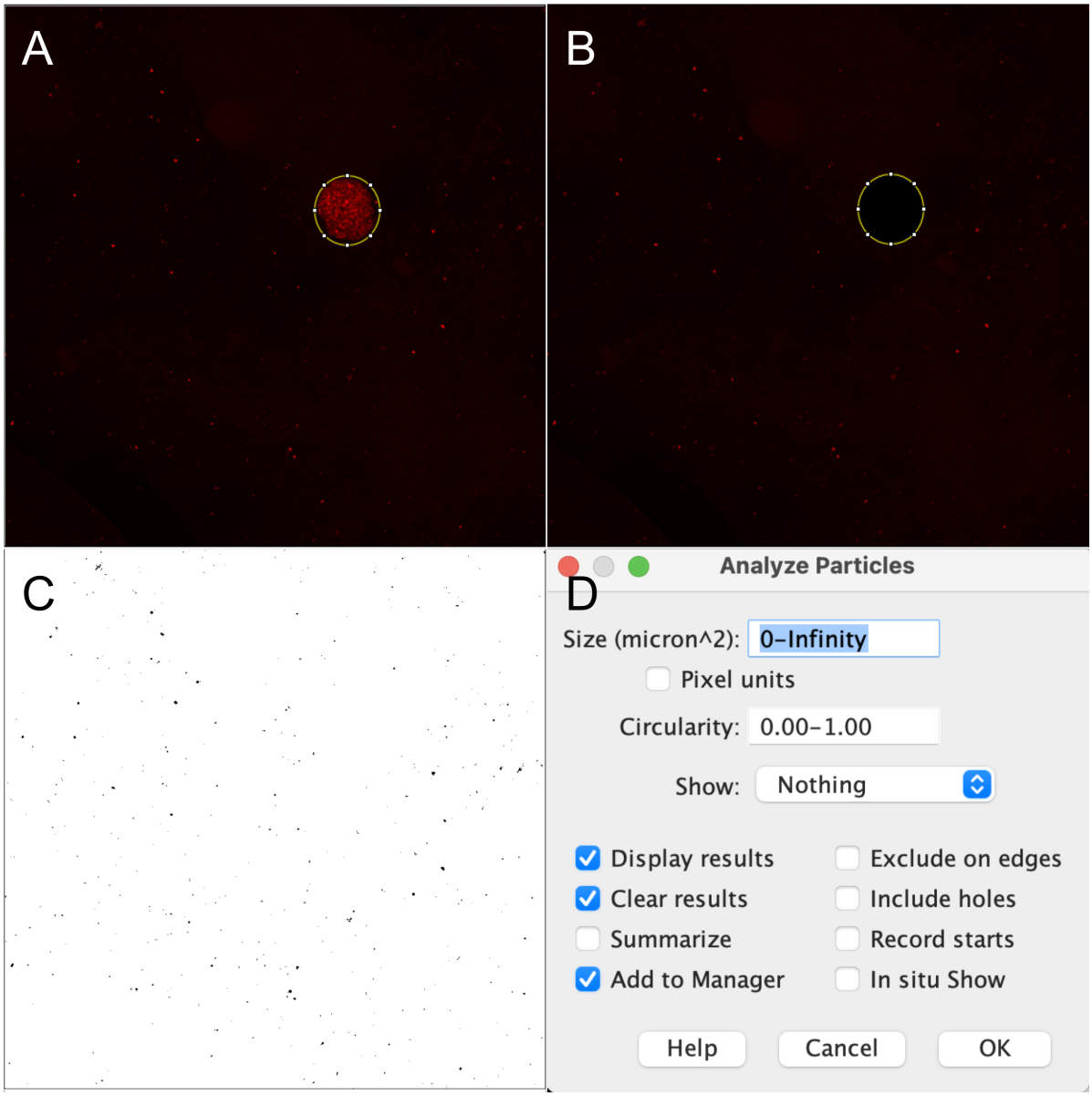

Figure 27 The area of interest was selected (A) and deleted (B) for the removal of aggregated cells from cell counting. Threshold (C) was set for further analysis using the analyze particles plugin (D).

D. Initial screening of cell-biomaterial interactions on disks

The processed CLSM images from the initial 24-hour screening are shown in Figure 28. CLSM was used to examine the morphology and spreading of NHDF cells seeded on top of crosslinked bioink gel disks composed of RGD coupled alginate combined with LHS-3 or Pro22 and mixed with TTC+M at 70/30 and 80/20 ratios. This method was used to investigate cell-biomaterial interactions to determine if the cells adhered to the scaffolds.

The stained cytoskeletons in all four images revealed elongated and spindle-shaped cells that interact with the bioink and with one another. This showed that cells had attached to all four bioinks and had spread to form ECM. Similar patterns for cell spreading and interactions were observed for LHS-3-*7030*RGD, LHS-3-*8020*RGD, and Pro22-*7030*RGD, whereas Pro22-*8020*RGD apparently showed fewer adhered cells but with similar morphology as for the other bioinks.

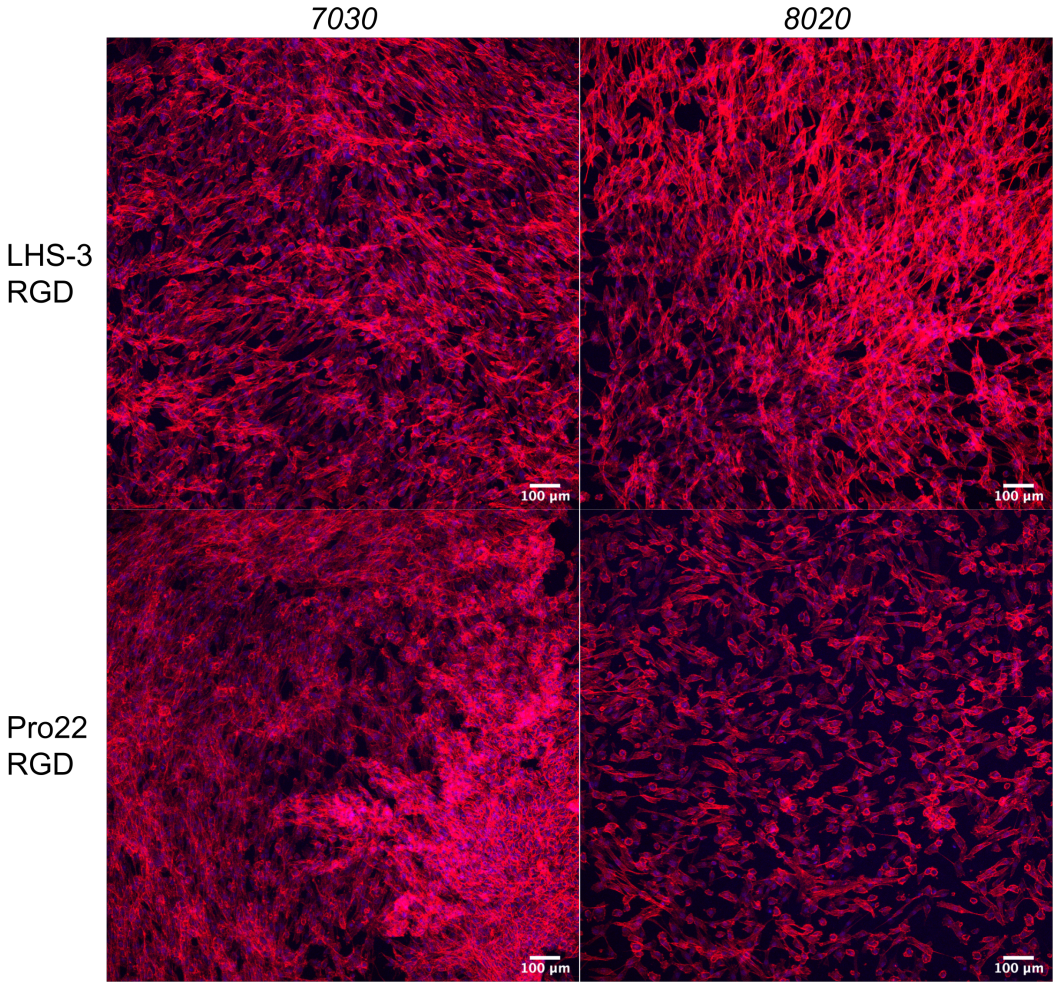

Figure 28 Processed CLSM images of NHDF cells stained with 568 phalloidin (red) and DAPI (blue) seeded on top of four different crosslinked bioink disks. Labels on top (*70/30* and *80/20*) refers to the alginate-TTC+M ratio of the bioinks. Labels on the left (LHS-3 RGD and Pro22 RGD) refers to the alginates used to formulate the bioinks. Scale bars correspond to 100 µm.

E. Scaffolds seeded with NHDF cells before relocation to new wells

Figure 29 shows CLSM images of stained NHDF cells seeded on scaffolds composed of eight different bioinks after 48 hours incubation before they were relocated into new wells. The dark areas were contours of the scaffolds, while the cytoskeleton and nucleus of the cells had merged into a purple color. Cells had attached to all four scaffolds while demonstrating an elongated and spindle-shaped morphology. Pro22*8020*RGD had an overexposed brightfield, making investigation of cell-biomaterial interactions more challenging. Despite the overexposure, some cell attachment was indicated at the interface between scaffold and well bottom. Because it was hard to differentiate whether the cells had adhered to the scaffold or the well bottom in all four images, the scaffolds were gently relocated into new wells as seen in Figure 21.

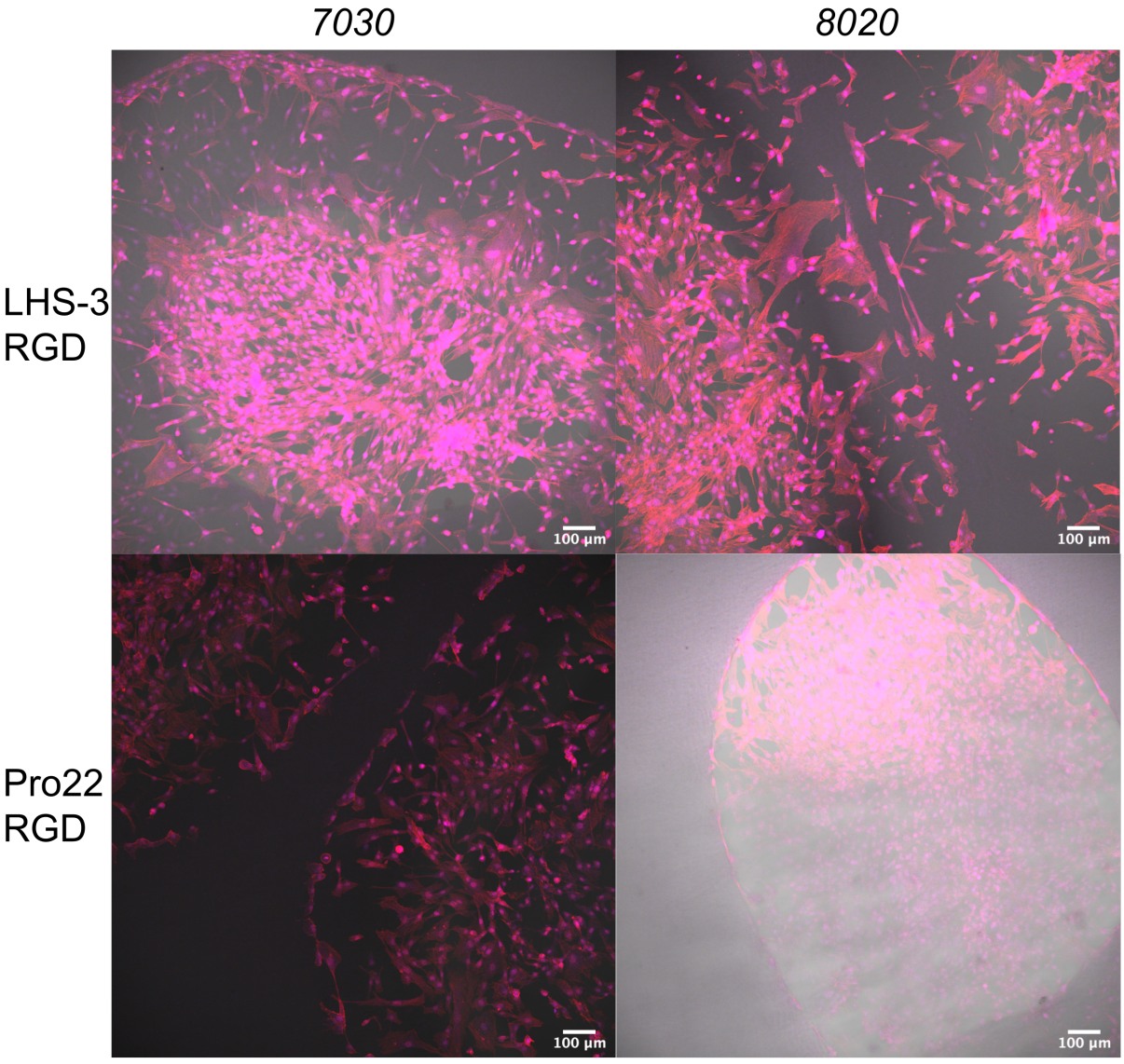

Figure 29 Processed CLSM images of the bioprints before they were relocated into new wells. The labels on top of the pictures refer to which alginate-TTC+M ratio (*70/30* or *80/20*) the bioinks were composed of. The labels to the left of the images refer to the type of alginate used (LHS-3 or Pro22) mixed with RGD coupled alginate (RGD). After incubation for 48 hours in a humidified incubator with 5% CO_2 and 37°C, cells were preserved and stained with Phalloidin and DAPI to excite the cytoskeleton (red) and nucleus (blue). Scale bars correspond to 100 µm.

F. 3D-view of long-term incubated NHDF cells seeded on scaffolds

Long-term incubated NHDF cells seeded on 3D-bioprinted scaffolds were examined for cell distribution in Fiji ImageJ. This revealed that the cells appeared to have grown on top of each other as layers in Figure 22 replicates B and D as seen in Figure 30 and Figure 31.

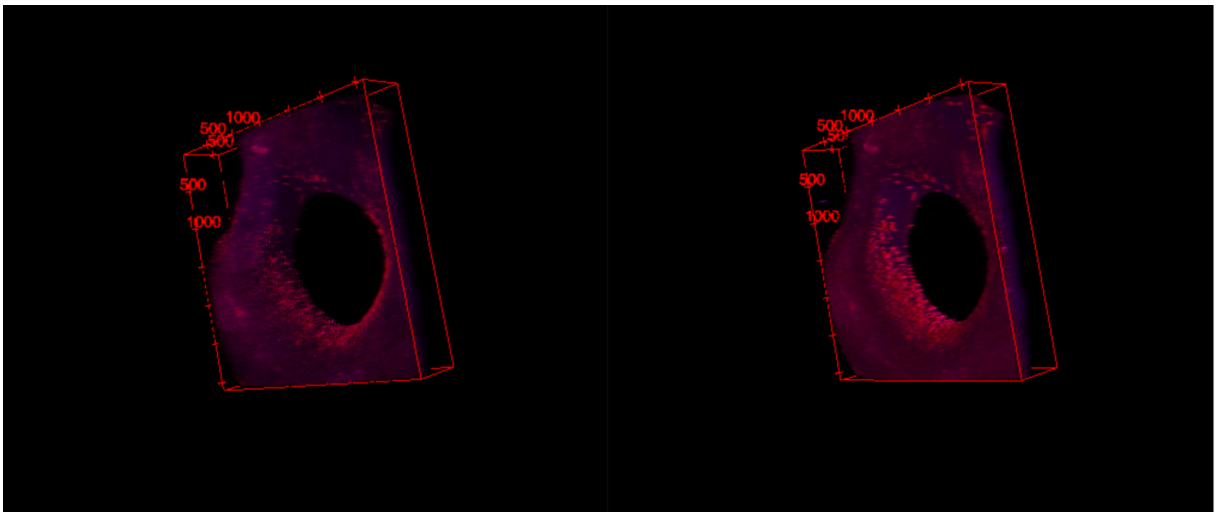

Figure 30 3D view of replica B from the long-term incubation of NHDF-cells seeded on bioprinted LHS-3-7030RGD. The nuclei and cytoskeletons were stained with Dapi and Phalloidin. Distribution of cells were examined and revealed that the cells had grown in top of each other. This was seen as layers in the 3D view as the image to the left is the bottom layer and the picture to the right reveals an upper layer of cells.

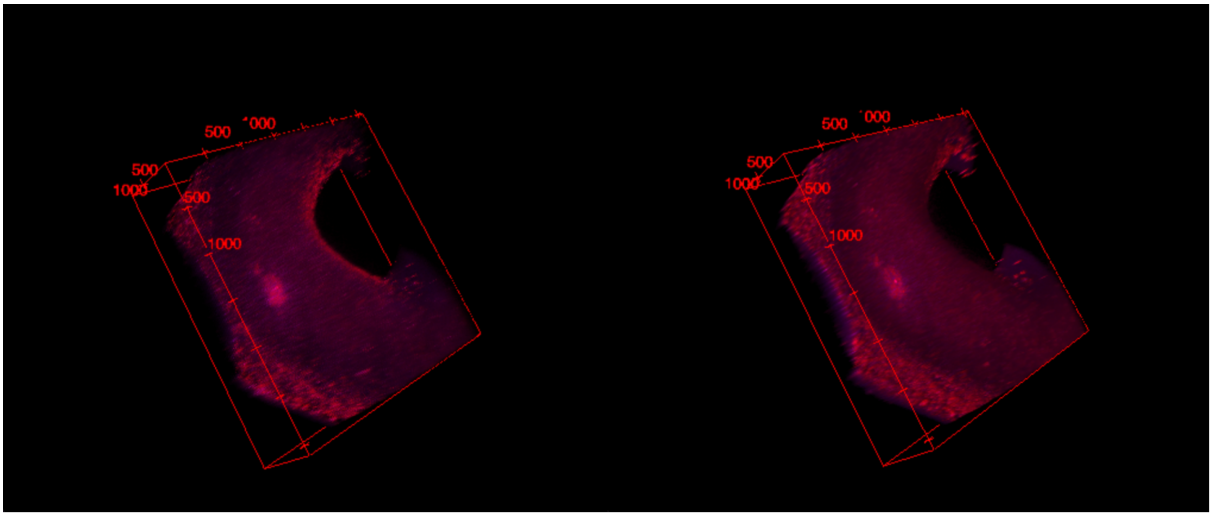

Figure 31 3D view of replica D from the long-term incubation of NHDF cells seeded on bioprinted LHS-3-7030RGD. The nuclei and cytoskeletons were stained with Dapi and Phalloidin. Distribution of cells were examined and revealed that the cells had grown in top of each other. This was seen as layers in the 3D view as the image to the left is the bottom layer and the picture to the right reveals an upper layer of cells.

G. Theoretical estimate of RGD molar concentration

Unmodified and RGD-coupled alginates were dissolved at 0.75% and 2.25% w/v in DMEM+. This was further mixed with TTC+M at 70/30 and 80/20 ratios resulting in a total alginate concentration of 0.9% and 0.6%. The w/v concentration of RGD-coupled alginate in the bioinks was therefore theoretically 0.675% and 0.45%. Molecular weight of the monomers in the alginate polymers were estimated to 198 mg/mmol. The alginates were 8% oxidized and substituted with 5% GRGDSP. A theoretical estimate of the RGD molar concentration was calculated using following equation:

$$Degree\ of\ substituted\ RGD * \frac{RGD\ coupled\ alginate\ concentration\ \left(\frac{mg}{mL}\right)}{Monomer\ weight\ \left(\frac{mg}{mmol}\right)} = Mole\ concentration\ of\ RGD\ (\frac{mmol}{mL})$$

RGD concentration in 70/30 ratios:

$$0.05 * \frac{6.75\frac{mg}{mL}}{198\frac{mg}{mmol}} = 1.7\ x\ 10^{-3}\ \frac{mmol}{mL} \rightarrow \underline{1.70\ \text{mM}}$$

RGD concentration in 80/20 ratios:

$$0.05 * \frac{4.5\frac{mg}{mL}}{198\frac{mg}{mmol}} = 1.5\ x\ 10^{-3}\ \frac{mmol}{mL} \rightarrow \underline{1.50\ \text{mM}}$$

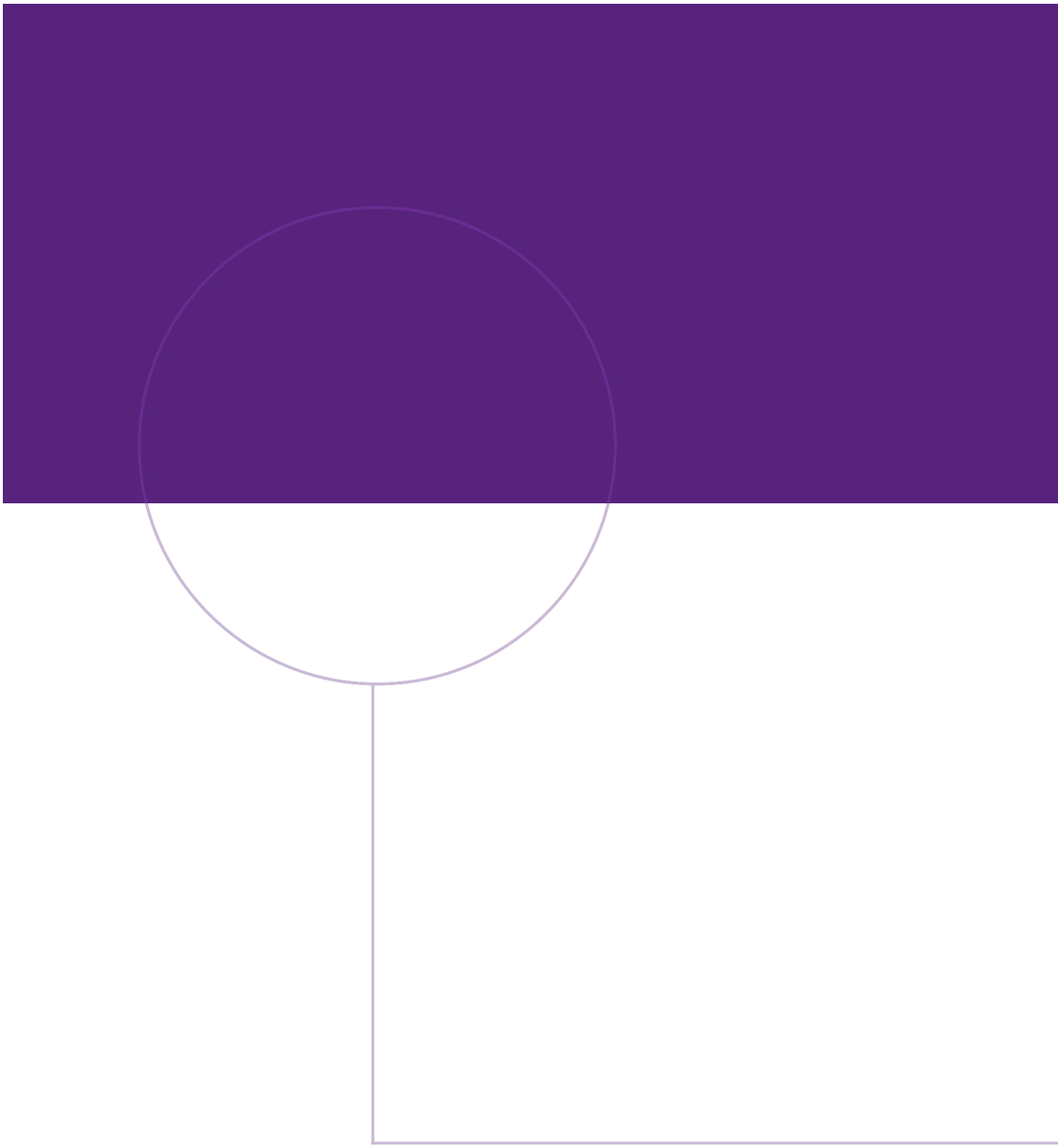

NTNU

Kunnskap for en bedre verden